

**Stress Dependence of the Burst Experiment for Determining Fracture Toughness**

by

**Yixuan Zhang**

B.S. Petroleum Engineering, China University of Petroleum, Beijing, 2017

Submitted to the Graduate Faculty of  
Swanson School of Engineering in partial fulfillment  
of the requirements for the degree of  
Master of Science in Petroleum Engineering

University of Pittsburgh

2019

UNIVERSITY OF PITTSBURGH  
SWANSON SCHOOL OF ENGINEERING

This thesis was presented

by

**Yixuan Zhang**

It was defended on

March 28, 2019

and approved by

Andrew P. Bunger, Ph.D., Associate Professor  
Department of Civil and Environmental Engineering  
Department of Chemical and Petroleum Engineering

Hseen Baled, Ph.D., Assistant Professor  
Department of Chemical and Petroleum Engineering

Robert Enick, Ph.D., Assistant Chair of Research,  
Department of Chemical and Petroleum Engineering

Thesis Advisor: Andrew P. Bunger, PhD, Associate Professor, Department of Civil and  
Environmental Engineering & Department of Chemical and Petroleum Engineering

Copyright © by Yixuan Zhang

2019

# Stress Dependence of the Burst Experiment for Determining Fracture Toughness

Yixuan Zhang, MS

University of Pittsburgh, 2019

The so-called “burst experiment” is used in the petroleum industry to measure the fracture toughness of reservoir rocks. It is considered advantageous compared to other methods because it tests rocks subjected to confining stress, which is more like field conditions. However, recent numerical simulations show that the burst experiment is possibly fundamentally dependent on the confining stress in a way which is not considered in the analysis of the experimental data. The reason is existence of a period of stable crack growth prior to the unstable “burst”. This stable growth is difficult to detect, and it raises large uncertainty in the crack length used in analysis of results.

In this thesis, a series of modified burst experiments with acoustic emission (AE) detection have been carried out to compare with predictions from modeling indicating that there will be stable growth for certain combinations of specimen geometry and loading, including the geometry most commonly used by industry. These tests give rise to evidence of stable growth before specimen rupture from two aspects. One is the difference between stable and unstable growth cases from AE records. The other is the behavior of calculated fracture toughness results. A criterion for spurious dependence of  $K_{IC}$  on confining stress for cases with stable growth is then specified based on stability of the specimen after failure. Also, the results of experiments using unstable configurations provide more self-consistent estimates of fracture toughness, most notably shown in a series of burst experiments with only unstable growth showing a positive correlation between fracture toughness and confining pressure, which is consistent with typical observations in the

literature. Finally, in other types of experiments with fixed confinement, a range of geometry and loading for valid calculation of  $K_{IC}$  is indicated based on the global stability criterion, providing guidance for improved design of this widely-used test method.

## Table of Contents

Preface.....	xi
<b>1.0 Introduction.....</b>	<b>1</b>
<b>1.1 Background.....</b>	<b>1</b>
<b>1.2 Literature Review.....</b>	<b>3</b>
<b>1.3 Motivations.....</b>	<b>11</b>
<b>1.4 Objectives.....</b>	<b>11</b>
<b>2.0 Theoretical Analysis.....</b>	<b>13</b>
<b>2.1 Problem Statement.....</b>	<b>13</b>
<b>2.2 Criterion of Global Stability.....</b>	<b>13</b>
<b>2.3 Fracture Toughness Estimation.....</b>	<b>15</b>
<b>2.4 Calculation of SIF.....</b>	<b>19</b>
<b>3.0 Experimental Method.....</b>	<b>23</b>
<b>3.1 Apparatus and Procedure.....</b>	<b>23</b>
<b>3.2 Specimen Preparation.....</b>	<b>27</b>
<b>3.3 Steps of Burst Experiment.....</b>	<b>31</b>
<b>3.4 Acoustic Emission Detection.....</b>	<b>32</b>
<b>4.0 Results of Experiments.....</b>	<b>34</b>
<b>4.1 Burst Experiments with <math>w=12</math>.....</b>	<b>34</b>
<b>4.1.1 Pressure Records.....</b>	<b>34</b>
<b>4.1.2 AE Records.....</b>	<b>36</b>
<b>4.2 Experiments with <math>w=3</math>.....</b>	<b>38</b>

4.2.1 Pressure Records.....	38
4.2.2 AE Records .....	41
4.3 Fixed Confinement Tests .....	44
5.0 Discussion.....	46
5.1 Estimates of Fracture Toughness.....	46
5.1.1 $K_{IC}$ Calculation.....	46
5.1.2 Configurational Dependence.....	48
5.2 Dependence of Fracture Toughness on Confinement .....	50
5.2.1 Stable Tests .....	50
5.2.2 Unstable Tests.....	52
5.2.3 Fixed Confinement Tests .....	54
5.3 Summary of Recommendations .....	56
6.0 Conclusion .....	57
Bibliography .....	59

## List of Tables

Table 1: Design of burst experiments (the “Stability” column is based on rw criterion, see Equation 3). .....	26
Table 2: Design of fixed confinement tests (the “Stability” column is based on rw criterion, see Equation 3).....	26
Table 3: Properties of Kasota Valley Limestone (from <i>Coldspring Quarry</i> , retrieved on March 3 from <a href="https://www.coldspringusa.com/quarry">https://www.coldspringusa.com/quarry</a> ) . .....	28
Table 4: Materials properties of Kasota Valley Limestone (from <i>Lu, 2018</i> ).....	28
Table 5: Summary of parameters and $K_{IC}$ calculation for all tests (note stability is determined by “rw” criterion, see Equation 3; “AE” means this test is under AE detection). .....	47
Table 6: Summary of parameters and $K_{IC}$ calculation for fixed confinement tests. ....	47

## List of Figures

Figure 1: Published results of fracture toughness versus confining stress on Indiana Limestone (after <i>Roegiers, 1991; Thallak, 1993; Abou-sayed 1978; Schmnidt, 1976</i> ).....	2
Figure 2: Schematic diagram of Griffith Theory (after <i>Griffith, 1924</i> ).....	3
Figure 3: Schematic of (a) single-edge test; (b) three-point bend test. (after <i>Schmidt and Huddle, 1976</i> ).....	5
Figure 4: Cross section of the apparatus for burst experiment (after <i>Abou-Sayed, 1978</i> ).....	6
Figure 5: Schematic of CDISK (after <i>Roegiers and Zhao, 1991</i> ).....	7
Figure 6: Apparatus of test (after <i>Thallak et al., 1993</i> ) .....	8
Figure 7: Apparatus of confined short beam compression test (after <i>Ko and Kemeny, 2007</i> ). .....	9
Figure 8: $K_{IC}$ versus confining prssure for Flagstaff sandstone (after <i>Ko and Kemeny, 2007</i> ). .....	9
Figure 9: Schematic of burst experiment (after <i>Yoshioka et al., 2019, in preparation</i> ). .....	10
Figure 10: Stress intensity factor evolutions against the fracture length, (a) according to <i>Yoshioka et al. (2019, in preparation)</i> ; (b) according to <i>Abou-Sayed (1978)</i> . .....	18
Figure 11: Superposition of the burst SIF (after <i>Abou-Sayed, 1978</i> ). .....	20
Figure 12: Approximate superposition for analysis of the burst SIF (after <i>Abou-Sayed, 1978</i> ) ..	20
Figure 13: Simulation results of $K_I^*$ for $w=3$ .....	21
Figure 14: Simulation results of $K_I^*$ for (a) $w=12$ , (b) $w=3$ , for fixed confinement tests .....	22
Figure 15 (a) Apparatus design for burst experiment, (b) triaxial cell. ....	24
Figure 16: (a) spacers and specimen for tests, (b) tube to provide inner pressure and rubber plug for system sealing.....	25
Figure 17: (a) Core drilling, (b) wire saw. ....	29
Figure 18: (a) grinding, (b) 0.5-inch limestone specimen, (c) 0.5-inch specimen.....	30

Figure 19: (a) Acoustic Emission detection system, (b) sensors placed in the bottom spacer, (c) sensor distribution. ....	33
Figure 20: Pressure records for burst experiments with $w=12$ , (a) test 1 (unconfined), (b) test 2 (unconfined), (c) test 3 ( $r=1/8$ ), (d) test 4 ( $r=1/6$ ), (e) test 5 ( $r=1/6$ ). ....	35
Figure 21: AE records corresponding to test 1 with $w=12$ , $r=0$ (predicted to has only unstable growth). ....	37
Figure 22: AE records corresponding to test with $w=12$ , $r=1/8$ (with predicted stable growth). .	37
Figure 23: Pressure records for burst experiments with $w=3$ (2-inch hole), (a) test 6 (unconfined), (b) test 8 ( $r=1/8$ ), (c) test 9 ( $r=1/6$ ), (d) test 10 ( $r=1/6$ ), (e) test 11 ( $r=1/6$ ), (f) test 12 ( $r=1/6$ ). ....	40
Figure 24: Specimen from test 12 after test with a third crack. ....	41
Figure 25: AE records corresponding to burst experiments with $w=3$ (a) $r=1/8$ (test 8), (b) $r=1/6$ (test 12). ....	43
Figure 26: Tests with fixed confinement as, (a) 1 MPa (test F-1), b) 3 MPa (test F-2), c) 4.8 MPa (test F-3). ....	45
Figure 27: Results of $K_{IC}$ calculation for all tests. ....	49
Figure 28: Results from burst experiment with $w=12$ , (a) $K_{IC}$ versus confining pressure, (b) $K_{IC}$ versus $rw$ (global equilibrium criterion, see Equation 2-3). ....	51
Figure 29: Results from burst experiment with $w=3$ , (a) $K_{IC}$ versus confining pressure, (b) $K_{IC}$ versus $rw$ (global equilibrium criterion, see Equation 2-3). ....	53
Figure 30: Results from fixed confinement tests, (a) $K_{IC}$ versus confining pressure, (b) $K_{IC}$ versus $rw$ (global equilibrium criterion, see Equation 2-3). ....	55

## Preface

Life is full of twists, I wish to express my wholehearted thanks to all the people who have illuminated the path and guided me into the right direction.

First and foremost, I would like to thank my advisor, Dr. Andrew Bungler, who provided me the opportunity to work in the group and work on a challenging research project. Thank you for guiding me into the lab and inspiring me a lot during analysis and organization of experimental results. Our numerous discussions are greatly helpful to me. Also, I was deeply impressed by your vivid Hydraulic Fracturing lectures, especially the fracturing models made by cartoons, which further stimulated my interests in this field.

Thanks also to the committee members, Dr. Enick, Professor Baled, and Dr. Bungler for making valuable suggestions and improving my research.

I am grateful to my friends and colleagues in the group, Charles Hager (Scooter), Guanyi Lu, Delal Gunaydin, Wei Fu, Yunxing Lu, Qiao Lu, and Yao Huang. In particular, I want to thank Scooter and Guanyi who have helped me solving numerous issues during lab experiments. Your working experiences have taught me a lot. I appreciate the research discussions with you, and I hope our friendship will last forever.

Here, I want to thank my parents for raising me and always supporting me for any choice I made. I really cherish the environment filled with happiness with you.

Financial support from Chevron is gratefully acknowledged. I want to thank Jose I Adachi, Amr Ei-Fayoumi, Karim S Zaki, and Keita Yoshioka for discussions and review of my project. Your ideas and numerical simulations are substantial to this research.

## 1.0 Introduction

### 1.1 Background

The burst experiment (*Abou-Sayed 1978; Abou-Sayed and Jones 1979*) is an important technique utilized in the petroleum industry to estimate the fracture toughness of rocks subjected to stresses that simulate reservoir conditions. In common use, it involves applying radial confinement to the boundary of a cylindrical specimen with concurrent pressurization of an interior, axially-notched borehole. The outer and inner pressure is increased proportionally until the specimen bursts. In the original publications, a numerically-determined stress intensity factor (*Bowie and Freese, 1972*) gives a premise for subsequent stress intensity factor analysis (*Abou-sayed, 1978*). In their modeling, prior authors assume the in-plane lines of elastic symmetry of the orthotropic plate coincide with the x axis and y axis. Under this assumption, the stress intensity factor is defined by an Airy stress function for plane symmetric loading. Then, fracture toughness measurements of both shale and sandstone specimens were performed, leading to an observation that the fracture toughness can be increased substantially – by an order of magnitude or more – for rocks under confining pressure compared with the laboratory results of unconfined tests (*Yoshioka et al., 2019, in preparation*). These burst experiments were carried out on thick-walled cylinder specimens with bi-wing notches for fracture initiation, and the steps of fracture toughness estimation followed. A combination of published results is shown in Figure 1, which indicates a positive relationship between the fracture toughness and the confining stress.

However, some recent numerical simulations (*Yoshioka et al., 2019, in preparation*) have demonstrated that the burst experiment could be fundamentally dependent on the confining stress

in a way which is not considered in the analysis of the experimental data. The modeling also predicts experiment modifications that will mitigate the spurious dependence on stress that in order to characterize the fracture toughness and actual variation with confining stress accurately. Hence the modeling leads to a two-fold working hypothesis. The first part of the hypothesis is that the current burst experiment is pseudo-dependent on the confining stress due to stable crack growth prior to the observed instability. The second part of the hypothesis is that a modified version will mitigate this issue and allow characterization of an accurate representation of the dependence of the fracture toughness on the confining stress.

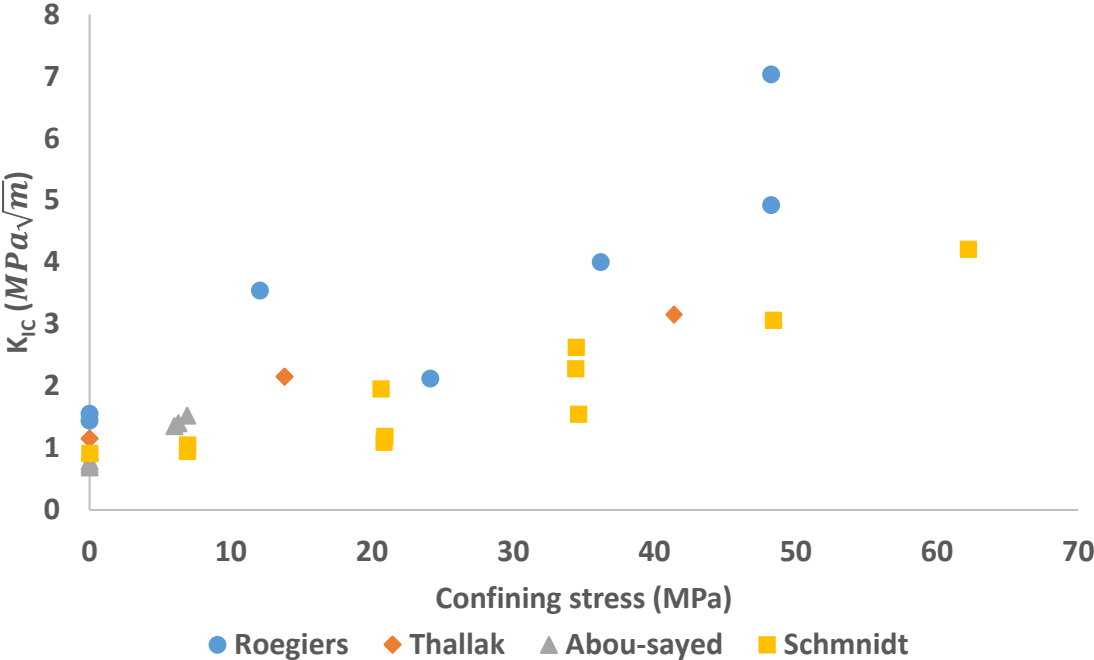


**Figure 1: Published results of fracture toughness versus confining stress on Indiana Limestone (after Roegiers, 1991; Thallak, 1993; Abou-sayed 1978; Schmmidt, 1976).**

## 1.2 Literature Review

*Griffith (1924)* proposed that a crack will propagate when the strain energy release rate that occurs due to crack growth is greater than or equal to the increase rate of effective surface energy due to the creation of new free surfaces, as is shown in Figure 2. This theory is applicable to elastic materials that fracture in a brittle fashion like glass. It depends on a critical energy release rate,  $G_c$ , which is supposed to be a material property. When loading is leading only to opening of the crack- not tearing or shearing- and when material damage is localized to a very small region near the crack tip, the energy criterion holds near equivalence to  $K_I = K_{IC}$  (*Irwin, 1957*), where  $K_I$  is the computed stress intensity factor and  $K_{IC}$  is the fracture toughness. Note  $K_{IC} = \frac{E' G_c}{\gamma_c}$ , where  $E' = \frac{E}{1-\nu^2}$  for Young's modulus  $E$  and Poisson's ratio  $\nu$ .

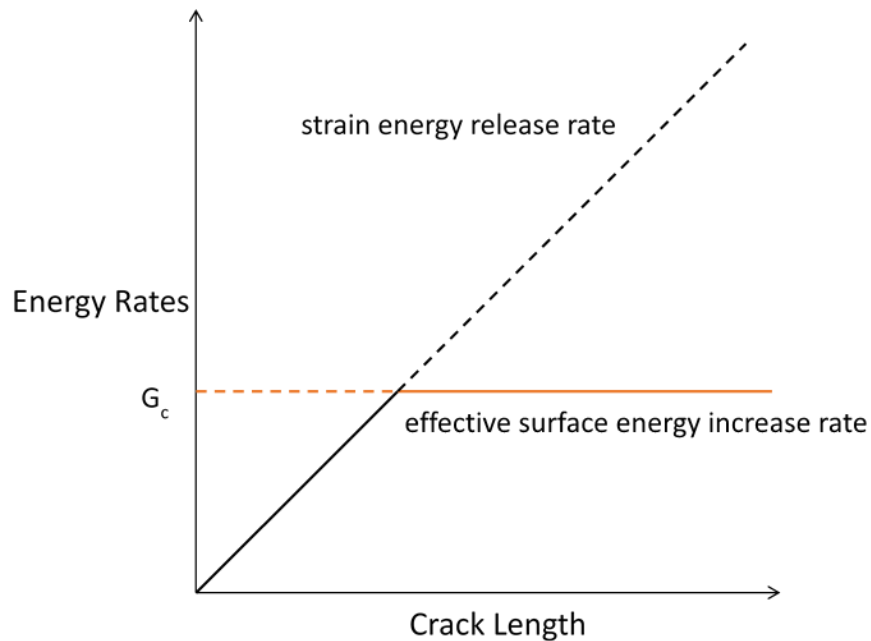


**Figure 2: Schematic diagram of Griffith Theory (after *Griffith, 1924*).**

The theory of fracture based on small deformation and small-scale plasticity is known as Linear Elastic Fracture Mechanics (LEFM). It is used in the calculation of  $K_{IC}$  and the condition of propagation  $K_I = K_{IC}$ . Based on LEFM, crack growth conditions are estimated by comparing the stress intensity factor and comparing it against the measured fracture toughness of the material. In turn,  $K_{IC}$  can be estimated by experiments using the computed critical stress intensity factor taken at the time of crack extension.

Where  $K_{IC}$  is supposed to be a constant material property, for rocks it is observed to depend on loading and geometry. For example, *Schmidt and Huddle (1976)* carried out experiments to study the effect of confining stress on fracture toughness of Indiana Limestone. They designed two types of experiments, namely, a single-edge-notch configuration (Figure 3a) and a three-point-bend setup (Figure 3b). According to the experimental results, they concluded that the fracture toughness can indeed vary as a function of the confining pressure. In the experiments with confinement up to 62 MPa, there was a linear positive correlation between the fracture toughness and the confining stress (see Figure 1).

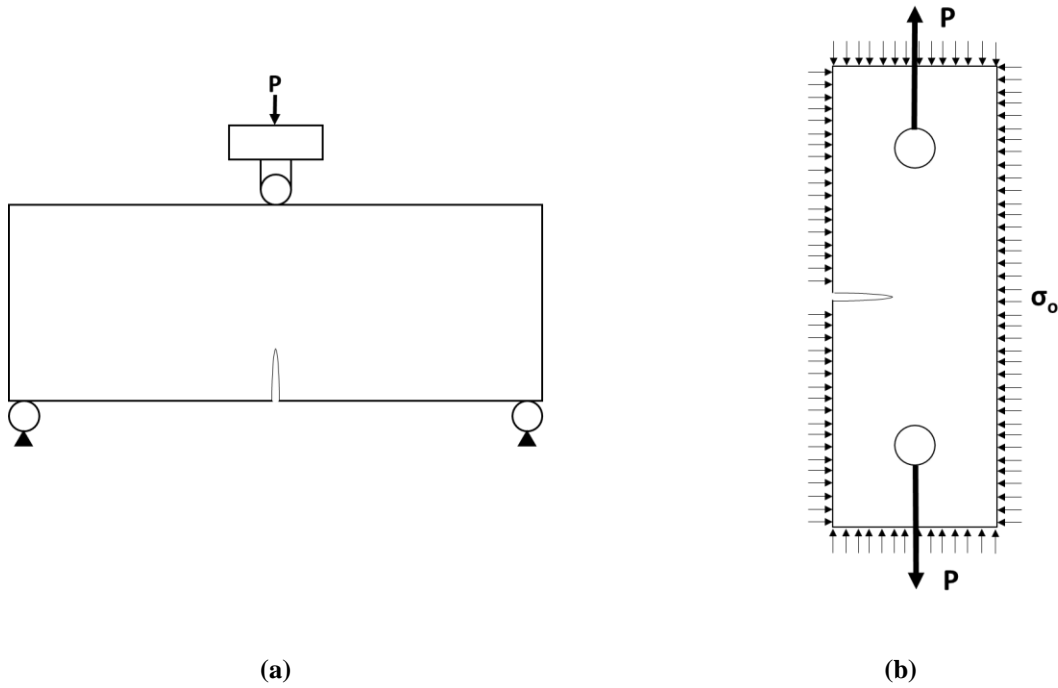


**Figure 3: Schematic of (a) three-point bend test; (b) single-edge test (after *Schimdt and Huddle, 1976*).**

To accurately represent the downhole conditions in petroleum reservoir, *Abou-Sayed (1978)* designed the burst experiment (see Figure 4) to accurately estimate the fracture toughness of specimens under confinement in a laboratory setting. Moreover, he put forward an analysis method based on fracture mechanics. He modified the evaluation process of  $K_{IC}$  for a confined cylinder specimen to be the superposition of a jacketed specimen and an unjacketed specimen. In his model, the fracture toughness was computed as the product of a non-dimensional stress intensity factor (determined by the initial notch length and geometric loading configuration), inner pressure, and square root of  $\pi a$  ( $a$  is the radius of the borehole). Their results are shown in Figure 1, in which there is a positive correlation between  $K_{IC}$  and confining stress.

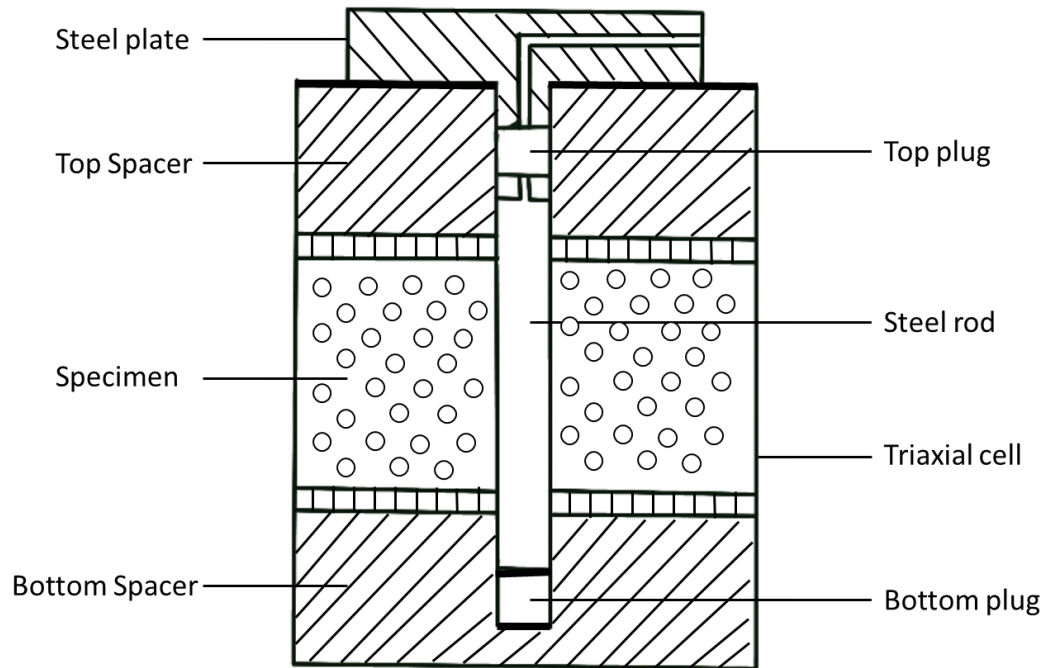


**Figure 4: Cross section of the apparatus for burst experiment (after *Abou-Sayed, 1978*)**

*Roegiers and Zhao (1991)* have carried out laboratory experiments to measure  $K_{IC}$  of rocks under simulated reservoir conditions. In their experiments, the Chevron-notched disk specimen (CDISK) is conducted in the load cell, which is shown in Figure 5. Here,  $P$  is the primary loading applying to the specimen, and the confining stress is supplied by hydraulic oil. The data generated from their tests are shown as a part of Figure 1. In general, they find the values of  $K_{IC}$  are significantly higher than previously published results. But the relationship between  $K_{IC}$  and confining pressure is again linear, which is broadly consistent with other works presented in Figure 1.

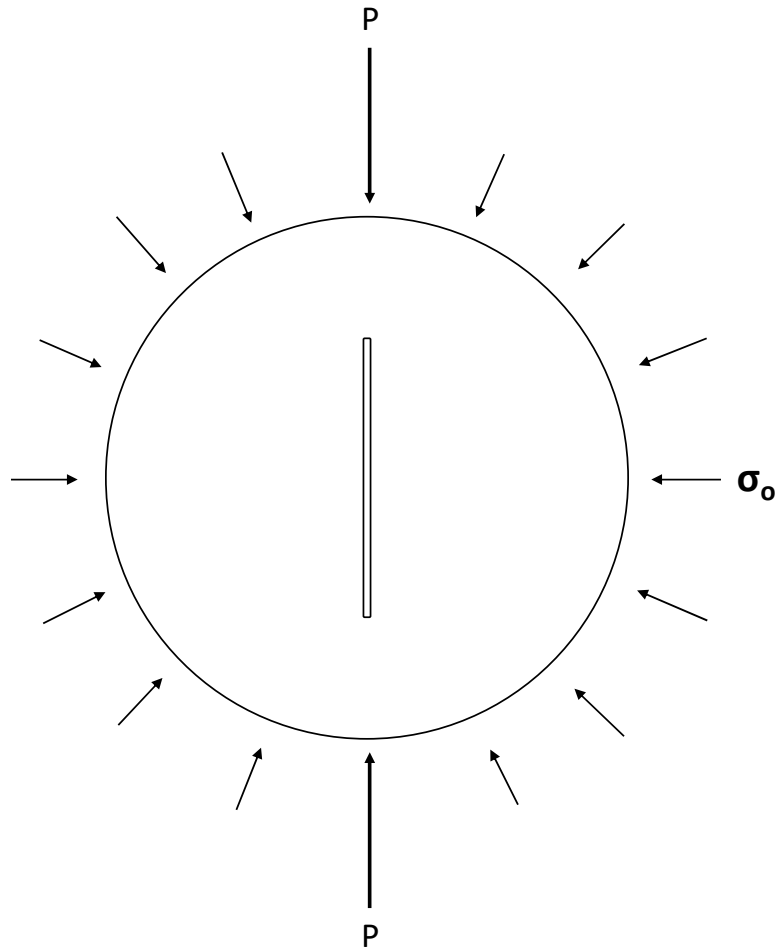


**Figure 5: Schematic of CDISK (after Roegiers and Zhao, 1991).**

*Thallak et al. (1993)* designed and carried out a series of experiments to measure fracture toughness in a hydraulic fracturing-like environment. The schematic drawing of their tests is shown in Figure 6, wherein they put the specimen into a cylindrical cell and then inject fracture fluid until evidence for crack growth or fracture break-through is observed. The confining stress is provided by fluid in the chamber and isolated from flowing into the specimen by the surrounding membrane. They also used LEFM to estimate the fracture toughness and all the results are

presented in the Figure 1. There is again a positive relationship between  $K_{IC}$  and confining pressure for Indian Limestone.

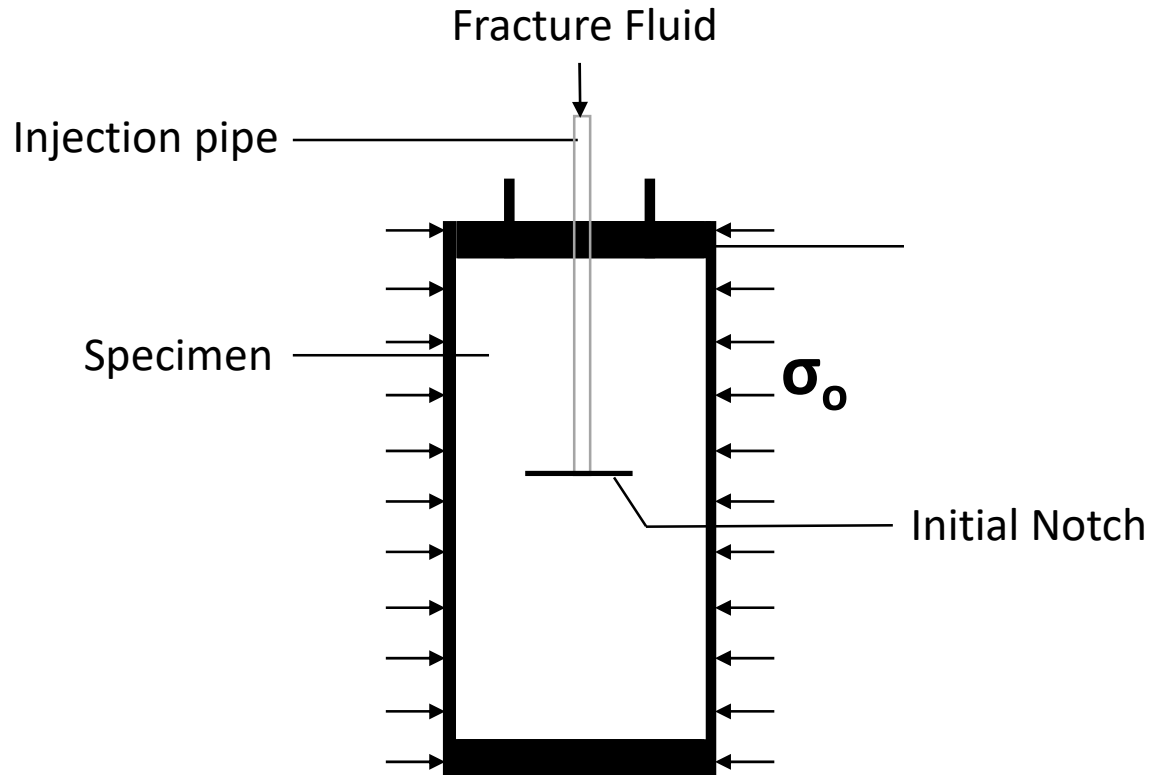


Figure 6: Apparatus of test (after *Thallak et al., 1993*)

*Ko and Kemeny (2007)* analyzed the dependence of fracture toughness on confinement and loading rate by carrying out a beam test with Flagstaff sandstone. The apparatus of this confined beam test is shown in Figure 7. The compressive load is applied from the platen on the top of the specimen. And the confining stress is applied from the surrounding cell. An elasto-plastic behavior or micro-cracking at the crack tip was considered in their model. Their experiment results also showed  $K_{IC}$  had proportional relationship with the confining stress (Figure 8).

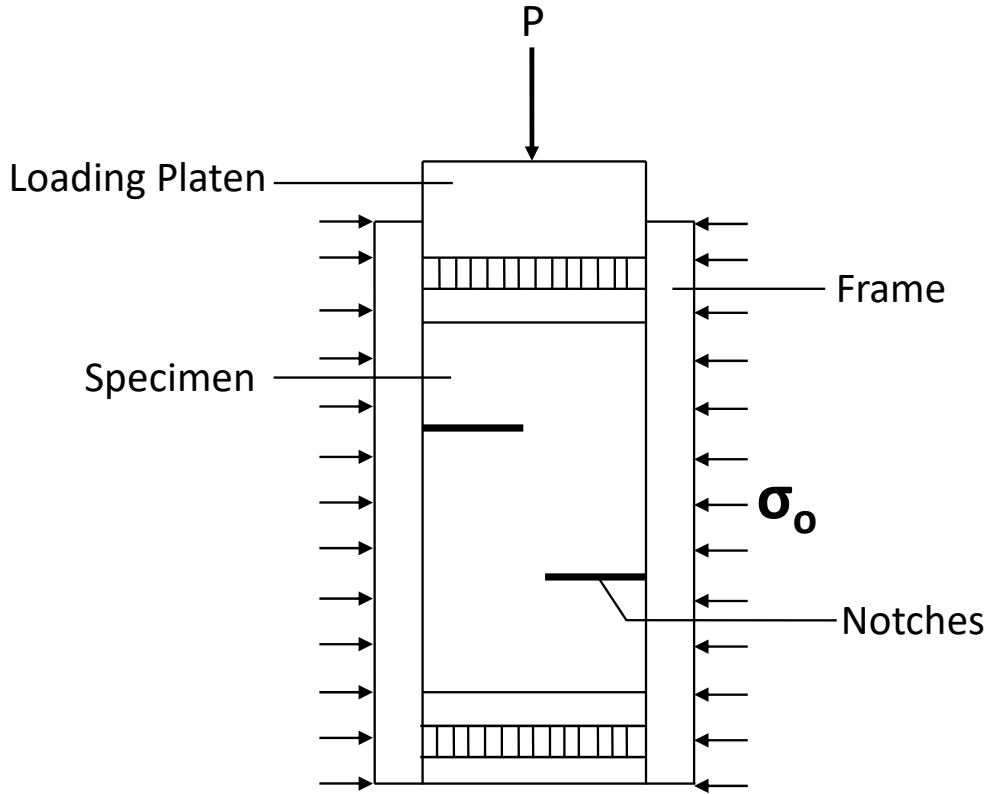


Figure 7: Apparatus of confined short beam compression test (after *Ko and Kemeny, 2007*).

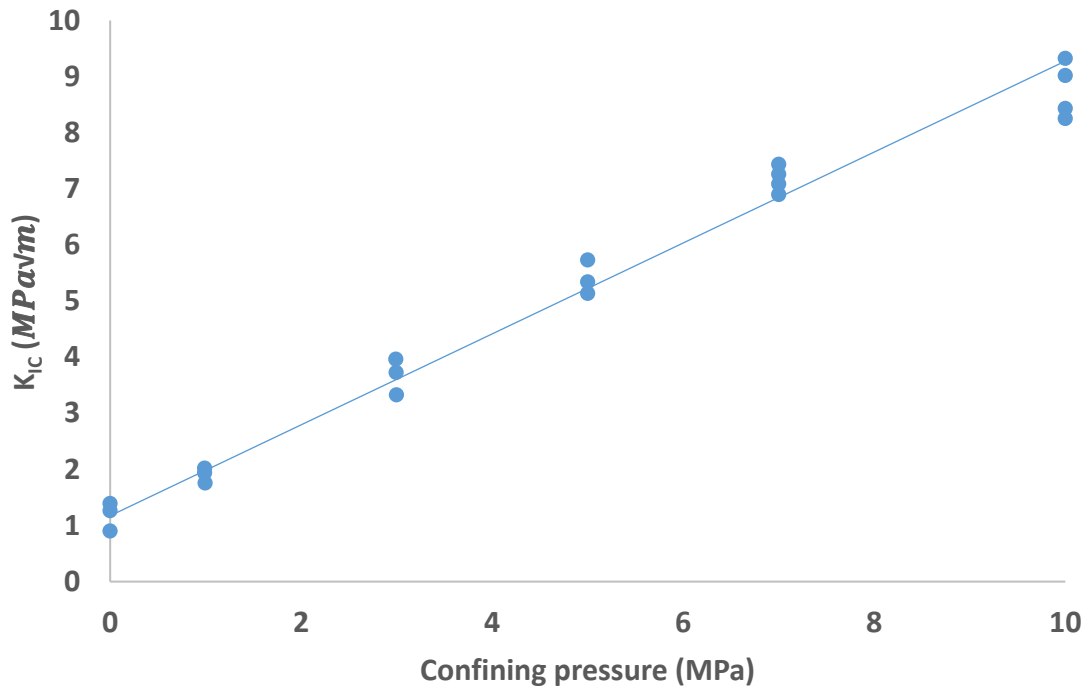


Figure 8:  $K_{IC}$  versus confining pressure for Flagstaff sandstone (after *Ko and Kemeny, 2007*).

Recent research by *Yoshioka et al. (2019, in preparation)* revisited the burst experiment analysis. They predict that the crack tip will extend into regions of compressive stress in some cases. This is a problem because it means that the crack length at the time of the global instability (the “burst”) will be longer than the assumed value of  $l_0$  (Figure 9). This inaccuracy in the crack length will lead to inaccurate interpretation of  $K_{IC}$ . Hence, they propose that there will be a possible stable growth before rupturing if the burst experiment has certain geometry and loading pressure ratios, and in these cases, there will be inaccurate estimation of the fracture toughness.

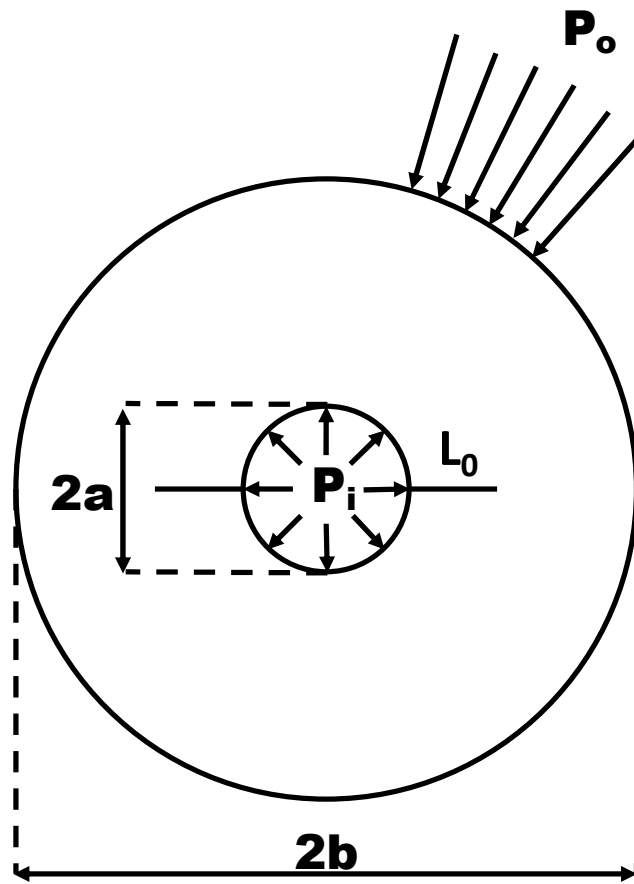


Figure 9: Schematic of burst experiment (after *Yoshioka et al., 2019, in preparation*).

### 1.3 Motivations

Previous research has studied the dependence of rock fracture toughness on confinement using different experiments, including single-edge-notch test, three-point-bending test, CDISK configuration test and beam test (recall in Section 1.2). These tests indicate fracture toughness is positively correlated to confining stress. However, the recent simulations of *Yoshioka et al. (2019, in preparation)* observed some potential inaccuracy of fracture toughness measurements when using burst experiment, a test which is thought to better simulate the petroleum reservoir conditions. They propose a hypothesis that there is a stable crack growth period prior to the observed rupture, and they put forward a modified modeling for the stress intensity factor (SIF) estimation. Motivated by this prior work, this thesis presents results from burst experiments with various loading geometries and, in some cases, with Acoustic Emission (AE) detection in order to experimentally evaluate the dependence of both  $K_{IC}$  of rocks and of the burst experiment itself on the level of confining stress.

### 1.4 Objectives

The first objective of this research is to propose a simple criterion for the existence of a stable period of crack growth prior to global. This criterion is intended to be a straightforward way to predict the stability and aid design of both stable and unstable tests with certain combinations of specimen geometry and loading.

The second objective is to compare experimental behavior for both stable and unstable configurations. A series of experiments are thus designed to observe possible evidence in some

tests of stable stable growth using both Acoustic Emission (AE) detection and comparison of the estimated  $K_{IC}$  between stable tests and unstable tests.

The third objective is to analyze the dependence of  $K_{IC}$  on confinement in both burst experiments and fixed confinement tests.

## 2.0 Theoretical Analysis

### 2.1 Problem Statement

Consider a cylinder specimen centralized in a triaxial cell. The top view schematic is shown in Figure 9. There is a bi-wing initial notch along the wellbore. The inner pressure is applied inside the wellbore as  $P_i$  and the confining pressure  $P_o$  is applied to the exterior surface. The ratio of the inner pressure to the outer pressure is  $r$ , and the ratio of the outer radius to the inner radius is  $w$ , that is:

$$P_o = rP_i, \quad a = wb \quad (2-1)$$

At the beginning of burst experiment, the pressure is increased simultaneously and proportionally with  $r$  unchanged, until specimen ruptures. The pressure data is recorded, and the peak pressures are selected to estimate the fracture toughness via the method described later in this chapter.

### 2.2 Criterion of Global Stability

Classically, the analysis assumes that the crack grows unstably and so the rupture at the conclusion of the experiment is taken to imply growth of a crack with initial notch length  $L_0$  (Yoshioka *et al.*, 2019, *in preparation*). However, more recent analysis proposes that when the crack tip reaches into a compression area, the propagation will arrest, requiring further

pressurization to generate instability (*Yoshioka et al., 2019, in preparation*). When this happens, the actual crack length associated with rupture is longer than  $L_0$ , leading to an inaccurate estimation of the stress intensity factor and hence the fracture toughness. Therefore, it is proposed to modify analysis to account for this stable range of crack growth, firstly from the perspective of global force analysis. Consider that there are two driving forces acting on the specimen. One is the expansion force caused by the inner pressure, and the other is the compression force given by the confinement. The difference between the two forces determines the global forces acting on the specimen, which is defined as the difference between the internal and external forces via,

$$\Delta F = F_i - F_o = 2\pi a P_i - 2\pi b P_o \quad (2-2)$$

Once the crack propagates, there is no longer a resisting force provided by the strength of the rock. Hence, the sign of  $\Delta F$  determines if specimen failure will occur under globally stable or unstable conditions. That is to say, two types of global conditions can be classified, corresponding to positive or negative value of  $\Delta F$ , respectively. So, if  $\Delta F > 0$ , the resultant force is outwardly directed, which means in this range the specimen is unstable after crack growth. This is the condition where the crack length at the onset of instability is known ( $L_0$ ), thus enabling accurate estimation of fracture toughness. On the other hand, if  $\Delta F < 0$ , the resultant force points inward, which means the specimen is stable even after crack growth. This leads to a hypothesis that there will be stable crack growth, with subsequent rupture occurring for a longer crack length compared to  $l_0$ , and perhaps even with instability that is not associated with crack growth at all but instead just the rupture of the inner membrane. Hence, the global force analysis indicates a criterion for the existence of instability versus stability, and directly implies conditions where toughness measurement should be more or less reliable.

To simplify the criterion, the pressure ratio  $r$  ( $\frac{P_o}{P_i}$ ) and the radius ratio  $w$  ( $\frac{b}{a}$ ) are used. Substituting into Equation (2-2), the criterion based on global force equilibrium is given by,

$$rw < 1, \text{ (unstable condition)}$$

$$rw > 1, \text{ (stable condition)} \quad (2-3)$$

### 2.3 Fracture Toughness Estimation

Fracture toughness ( $K_{IC}$ ) is a property which describes the ability of a material to resist fracture. The development of linear-elastic fracture mechanics (LEFM) started with Griffith's research on glass. Fundamentally, the Griffith theory considers the energy changes associated with incremental crack growth (*Griffith, 1924*). Griffith postulated that the total potential energy of stressed solid body is related to the release of the stored energy and the work done by the external loads. Based on his theory, the fracture stress of glass can be predicted by using an energy balance equation, that is, the decrease of potential energy per unit thickness is equal to the increase of surface energy per unit thickness at the rupturing point, namely,

$$U = U_s + U_e \geq 0 \quad (2-4)$$

here,

$U_s$ : Elastic surface energy per unit thickness (J/mm).

$U_e$ : Released elastic energy per unit thickness (J/mm).

and,

$$U_e = V \int \sigma d\varepsilon, \quad U_s = 2L\gamma_s \quad (2-5)$$

Here,

$V$ : Volume of specimen ( $\text{mm}^3$ ).

$\sigma$ : Applied stress (MPa).

$\varepsilon$ : Elastic strain.

$L$ : Initial notch length (mm).

$\gamma_s$ : Specific surface energy for atomic bond breakage ( $\text{J}/\text{mm}^2$ )

The energy balance criterion can be simplified using Hooke's Law ( $\sigma = E'\varepsilon$ , where  $E' = \frac{E}{1-\nu^2}$ ) and the strain energy releasing rate ( $G_I = 2\gamma_s$ ), such as, the Stress Intensity Factor for a straight crack in an infinite domain where  $L$  is the crack length.

$$K_I = \sigma\sqrt{\pi L} \quad (2-6)$$

The critical value of stress intensity factor at which the crack extends is called fracture toughness, denoted  $K_{IC}$ . Stress intensity factor is therefore a function of stress and initial length. Equation (2-6) is valid for a straight crack subjected to uniform tension in an infinite homogeneous solid. A modified equation for the estimation of fracture toughness for the burst experiment configuration was firstly put forward by *Abou-Sayed (1978)* as

$$K_{IC}(l) = P_i K_I^B(1, l, w, r)\sqrt{a\pi} \quad (2-7)$$

$P_i$ : Inner pressure.

$K_I$ : Stress intensity factor.

$a$  : Radio of hole.

$r$  : Ratiuos of confining pressure over inner pressure.

$w$  : Ratio of outer diameter over inner diameter.

$l$ : Normalized crack length  $L$ , where  $l = \frac{L}{b-a}$ .

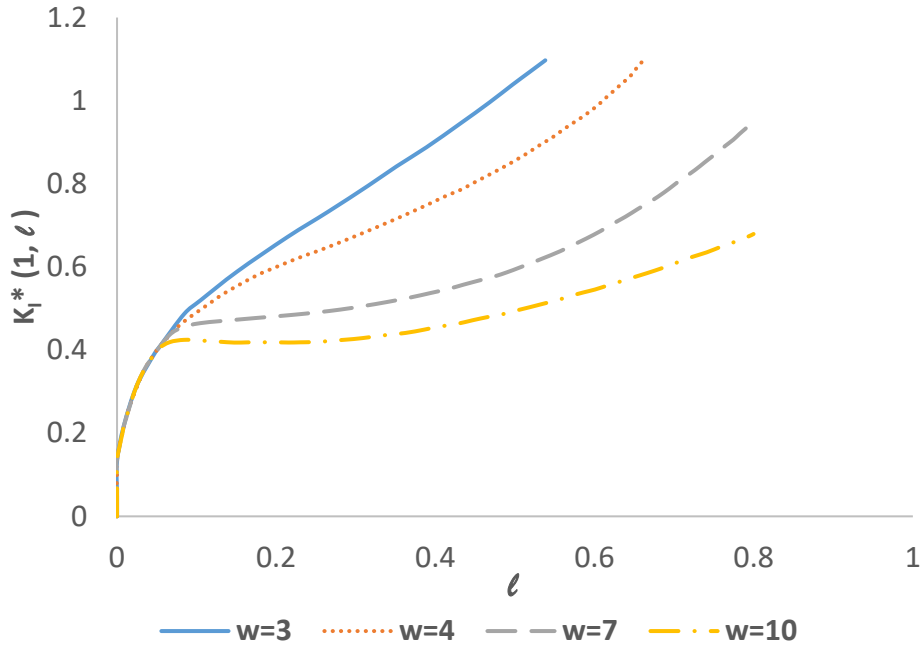
Here  $K_I^B$  is stress intensity factor normalized by  $\sqrt{a\pi}$  which can be numerically computed. The original calculation of *Abou-Sayed (1978)* is shown in Figure 10(b). During the estimating process of  $K_I$ , an important parameter is the initial length of the notch,  $L_0$ , given an initial value of the normalized crack length.

$$l_0 = \frac{L_0}{b-a} \quad (2-8)$$

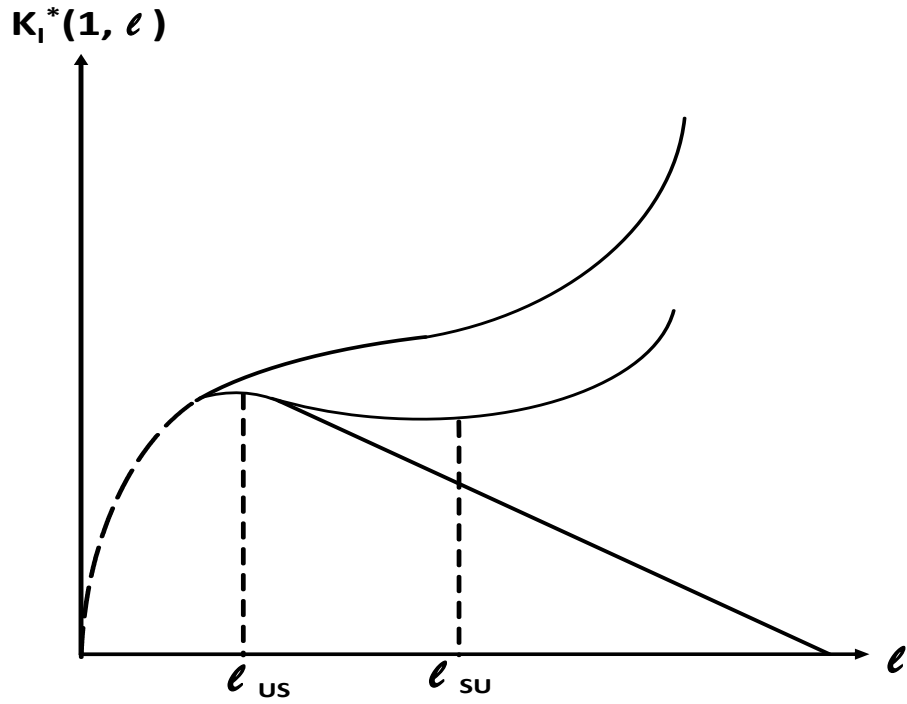
For the case of a thick-walled cylinder ( $w > 9$ ) and with confining pressure ( $r > 0$ ), the fracture growth may be stable as characterized in evolution curve, as shown in Figure 10(a). If the initial length of fracture is  $l_{US}$ , the fracture growth becomes stable as  $K_I^*$  decreases, hence  $P_i\sqrt{\pi a}K_I^*$  stays smaller than  $K_{IC}$  until the fracture growth becomes unstable again at the length  $l_{SU}$ . Therefore, the crack is predicted to grow stably after initiation if the value of  $l$  satisfies:

$$l_{SU} < l < l_{us} \quad (2-9)$$

Thus, the analysis is useful in two ways. Firstly, it provides the necessary computed value of  $K_I^B$  for estimation of  $K_{IC}$  using experimental data for specimen geometry and pressure at the time of failure. Secondly, it corroborates the global stability criterion, showing that a period of stable crack growth can exist for small enough  $l_0$  provided that  $rw > 1$ .



(a)



(b)

Figure 10: Stress intensity factor evolutions against the fracture length, (a) according to Yoshioka et al. (2019, in preparation); (b) according to Abou-Sayed (1978).

## 2.4 Calculation of SIF

During the estimation of fracture toughness, simulation for burst SIF is considered to be an important step. During this process, a method called G-theta (*Geniaut et al., 2005*) has been widely used to calculate the energy release rate after Griffith Theory proposing an energy balance method to analyze the fracture on glass as a brittle material. The G-theta is based on the estimation of second derivatives of the energy potential with respect to crack length using the technique of virtual domain perturbation theta. Numerically it uses an integral over a surface, which is more accurate than the contour integral used by the J-integral (*Rice et al. 1973*). Evaluate the normalized SIF or the energy release rate G are related using Irwin's formula (*Irwin, 1958*).

The first step is to decomposition Equation (2-7) into elementary problems. *Abou-Sayed, 1978* proposed a method to decomposed it into two problems: 1) the jacketed problem, in which the pressure applied only on the inner cylinder and 2) the problem C, in which the confining pressure only applied on the outer cylinder as shown in Figure 11. Therefore, calculation process of burst SIF can be superimposed as:

$$K_I^*(1, l, w, r) = K_I^{J*}(1, l, w) - rK_I^{C*}(1, l, w) \quad (2-10)$$

Our burst experiments use unsaturated rocks, which means pore pressure can be ignored ( $P_{pore} = 0$ ). The superposition can be utilized into another version with a new part calledunjacketed problem, shown in Figure 12:

$$K_I^*(1, l, w, r) = K_I^{J*}(1, l, w) - rK_I^{U*}(1, l, w) \quad (2-11)$$

This equation gives an approximate estimation of burst SIF, during which Jacket SIF and Unjacketed SIF can be simulated respectively.

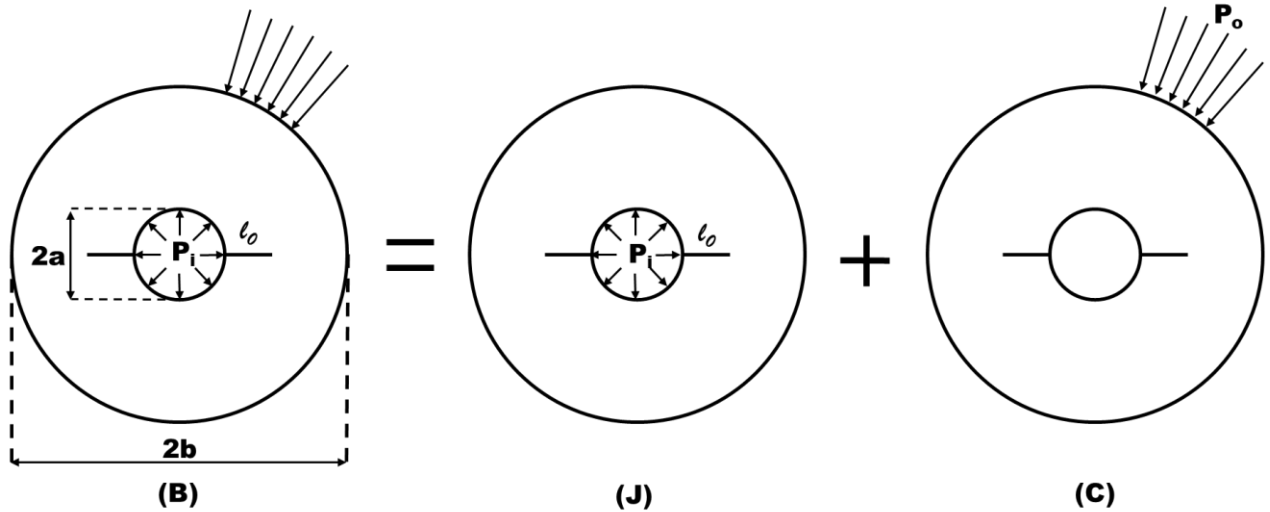


Figure 11: Superposition of the burst SIF (after *Abou-Sayed, 1978*).

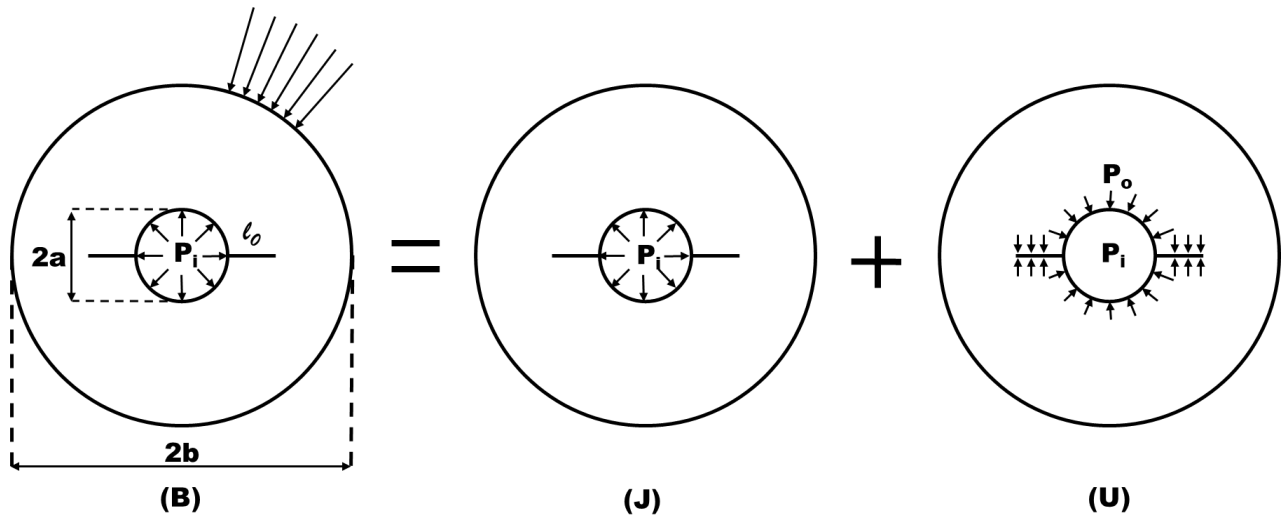


Figure 12: Approximate superposition for analysis of the burst SIF (after *Abou-Sayed, 1978*).

The SIFs are estimated by the G-theta method, which is based on the second derivatives of the energy potential with respect to crack length using the technique of virtual domain perturbation  $\theta$ . *Geniant and Massin (2005)* gives the detail of this process. Then the SIFs of both jacketed and unjacketed problems have been calculated using this method. Finally, the results from

superposition of these two SIFs is shown in Figure 13, 14. In these simulation results, the three types of relationship between normalized SIF and non-dimensional notch length are similar to these shown in Figure 13. When  $\frac{1}{r}$  is larger than  $w$  ( $rw < 1$ ), which means there is only unstable growth in these cases based on global force equilibrium criterion mentioned in Chapter 2,  $K_I^*$  is generally proportional to the initial notch length. If  $\frac{1}{r}$  is equal to or even smaller than  $w$  ( $rw > 1$ ), a downward period will occur in SIF simulation. It is possibly due to a pre-existing stable growth according to our hypothesis.

In order to calculate the fracture toughness with SIF simulation, the dimensionless initial notch length  $l$  is fixed as 0.11 for 0.5-inch tests and 0.15 for 2-inch tests. Therefore, the normalized value of  $K_I^*$  for each test can be estimated according to the simulation results as shown in Figure 13 and Figure 14, corresponding to the values of  $r$  and  $w$ . Based on these values and Equation (2-7),  $K_{IC}$  for each case can be estimated when the critical inner pressure can be obtained at the rupturing point during each burst experiment in following sections.

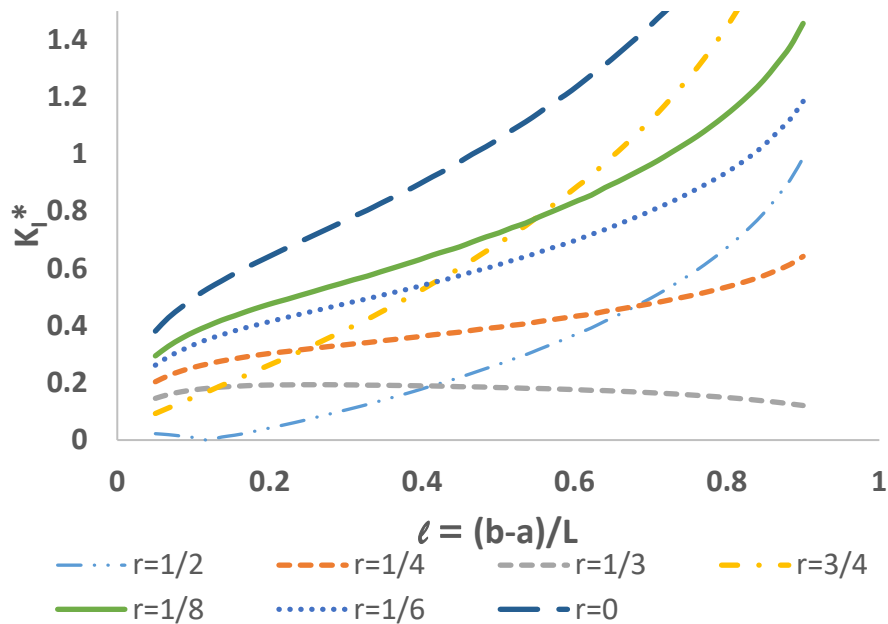
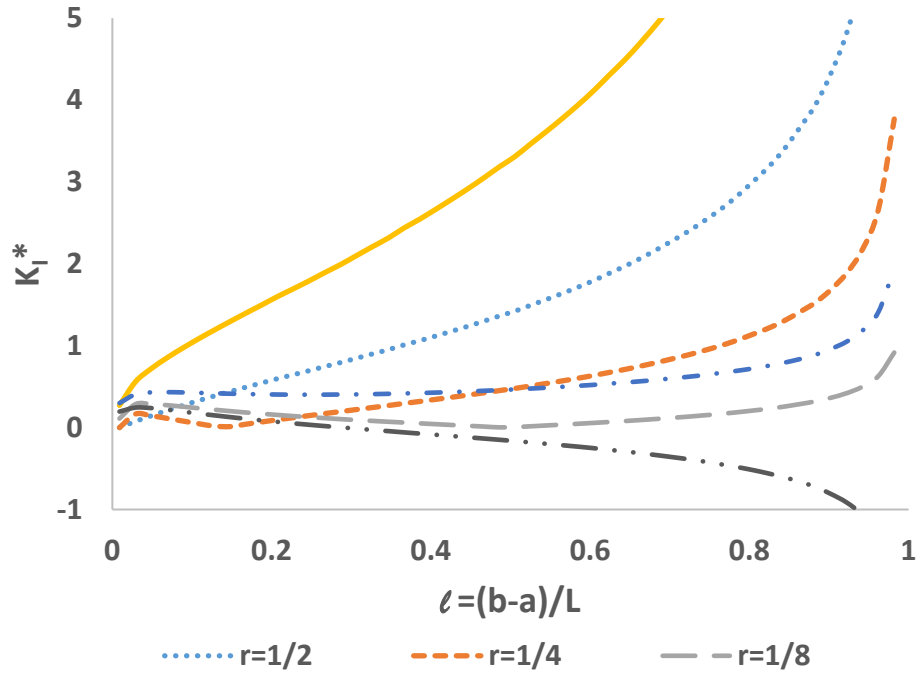
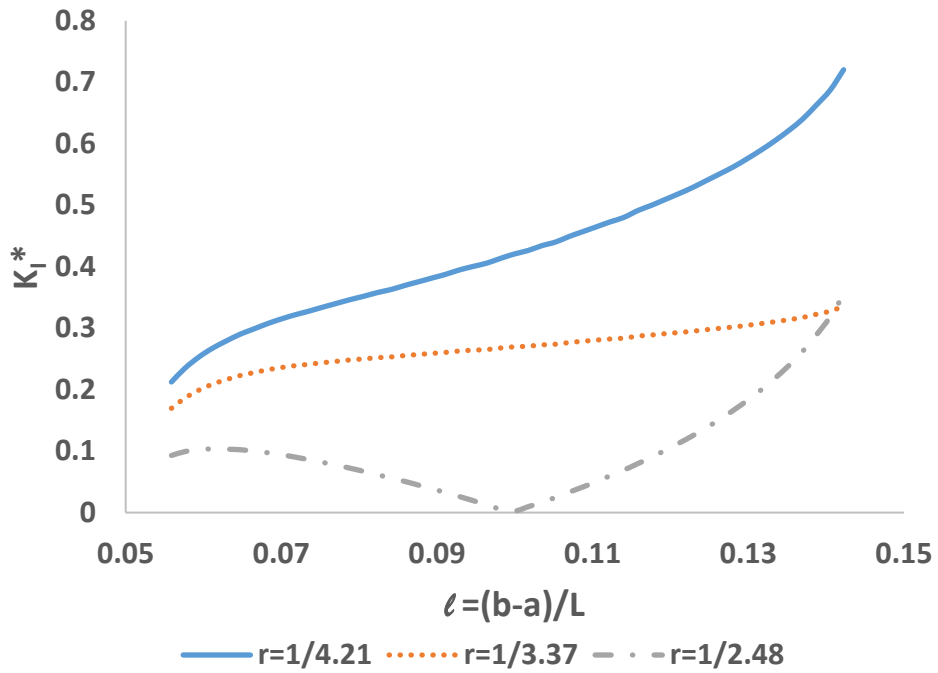


Figure 13: Simulation results of  $K_I^*$  for  $w=3$ .



(a)



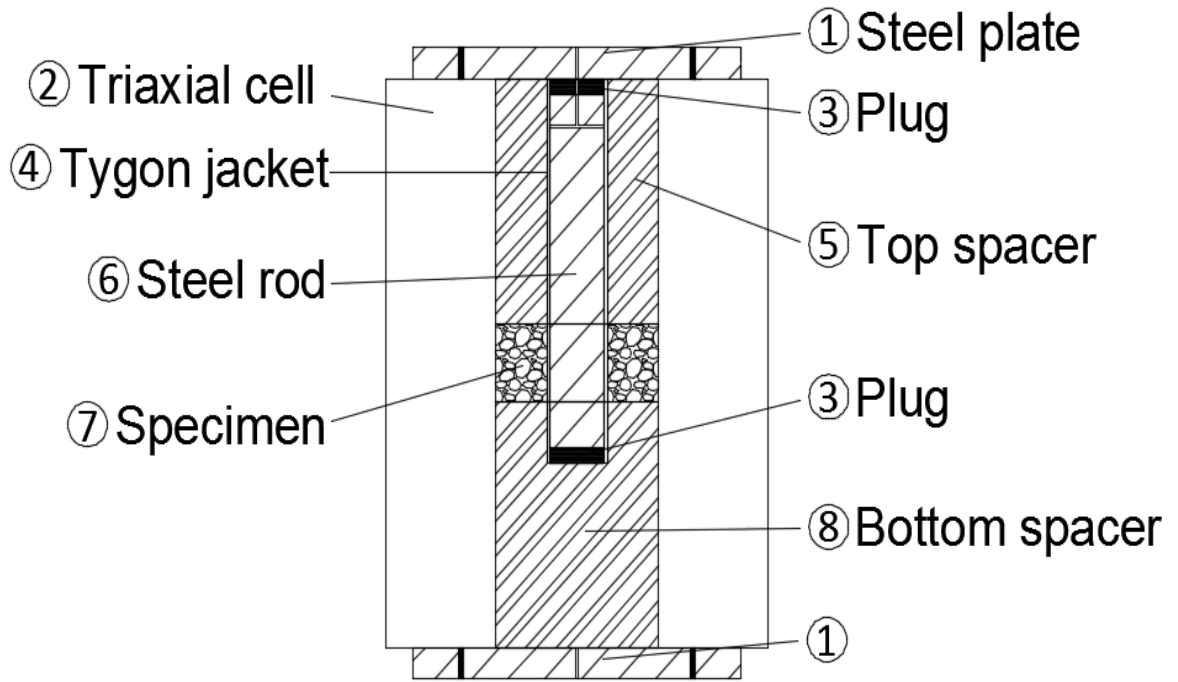
(b)

Figure 14: Simulation results of  $K_I^*$  for (a)  $w=12$ , (b)  $w=3$ , for fixed confinement tests

### **3.0 Experimental Method**

#### **3.1 Apparatus and Procedure**

The burst experiment set-up is shown in Figure 15(a). To begin a test, the cylindrical rock specimen is placed in the center of a triaxial cell, surrounded by the oil filled chamber providing the confining stress. The invasion of oil into the specimen is prevented by the outer membrane. The specimen is held at the vertical center of the cell by two aluminum spacers. A Tygon tube (Figure 16b) is inserted into the central hole of specimen and sealed by two rubber plugs. Inside the Tygon tube, the steel rod holds the two rubber plugs in place, expanding them via compression thereby providing better sealing. This system provides for application of the inner pressure while preventing fluid from infiltrating the specimen. The steel plate covers are held in place by bolts at the top and bottom to keep the system intact. Two ISCO syringe pumps are used simultaneously to ramp up both the inner pressure and the confining pressure until a pressure drop is observed.



(a)

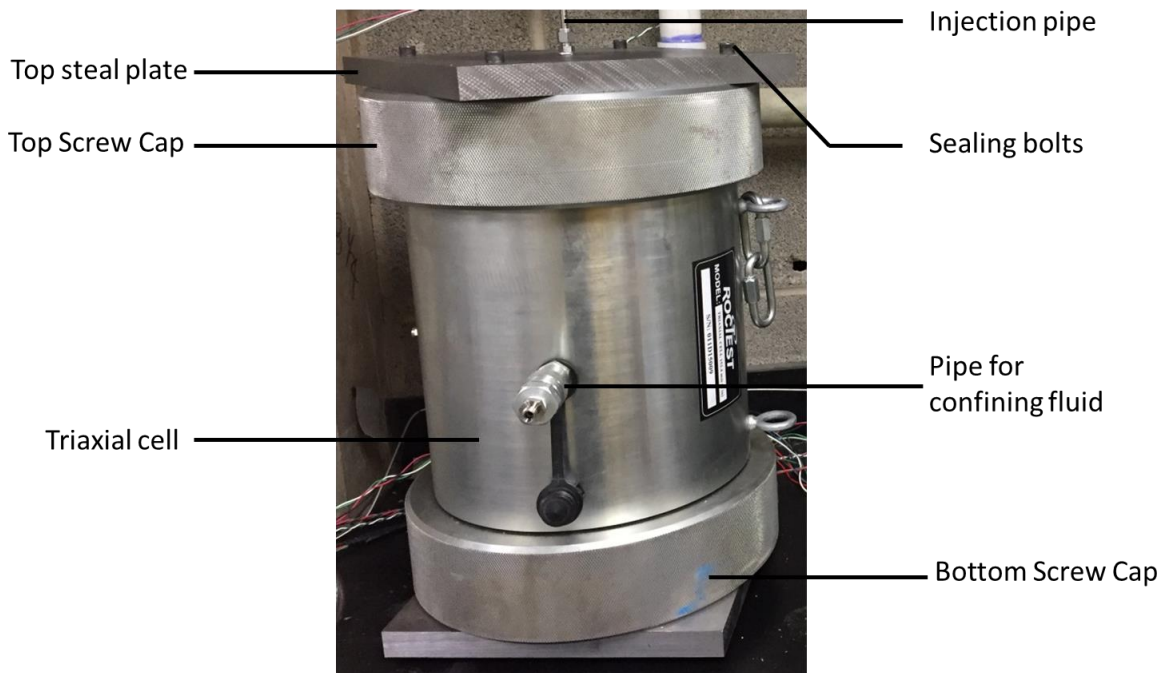
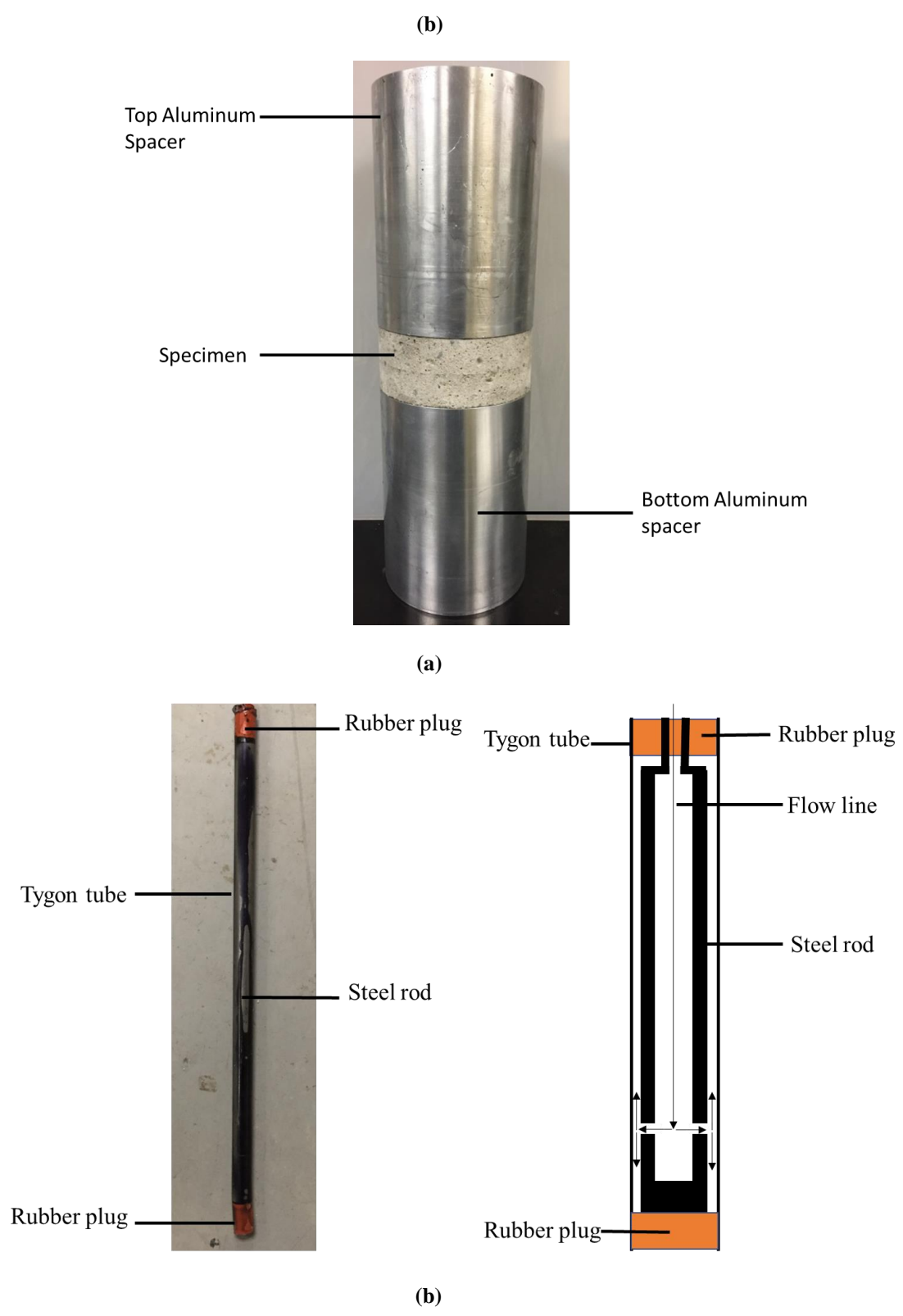


Figure 15 (a) Apparatus design for burst experiment, (b) triaxial cell.



**Figure 16: (a) spacers and specimen for tests, (b) tube to provide inner pressure and rubber plug for system sealing.**

The series of burst experiments is shown in Table 1 and Table 2. There are two kinds of hole sizes: 0.5 inch ( $w = 12$ ) and 2 inch ( $w = 3$ ). The values of the parameter  $r$  is chosen to be  $0, \frac{1}{6}, \frac{1}{8}$ . The stability is predicted based on global equilibrium criterion (Equation (2-3)).

**Table 1: Design of burst experiments (the “Stability” column is based on  $rw$  criterion, see Equation (2-3)).**

Test Name	Stability	Hole size (in)	$w=b/a$	$r=Po/Pi$	$rw$
1	unstable	0.5	12	0	0
2, AE	unstable	0.5	12	0	0
3, AE	stable	0.5	12	1/8	1.5
4	stable	0.5	12	1/6	2
5	stable	0.5	12	1/6	2
6	unstable	2	3	0	0
7	unstable	2	3	0	0
8, AE	unstable	2	3	1/8	0.375
9	unstable	2	3	1/6	0.5
10	unstable	2	3	1/6	0.5
11	unstable	2	3	1/6	0.5
12, AE	unstable	2	3	1/6	0.5

**Table 2: Design of fixed confinement tests (the “Stability” column is based on  $rw$  criterion, see Equation (2-3)).**

Tests Name	Stability	Fixed Po	$w$	$r$	$rw$
F-1	unstable	1	3.00	0.24	0.71
F-2	unstable	3	3.00	0.30	0.89
F-3	stable	4.8	3.00	0.40	1.21

### 3.2 Specimen Preparation

The burst experiment is performed with Kasota Valley Limestone, a dolomitic limestone found and quarried in southern Minnesota, especially near the Minnesota River and its tributaries. As a part of Oneota Dolostone Formation of Southern Minnesota, it has a long history of about 450 million years (lower Ordovician Period) (*Stauffer, 1933*). This type of limestone is commonly used in architecture since it is magnesium rich, making it more resistant to weathering compared to more calcium-rich limestone. Table 3 shows some physical properties of the limestone (test data from *Coldspring Quarry (2009)*). Also, Table 4 shows other properties of Kasota Valley Limestone from *Lu (2018)*, and also including fracture toughness obtained from *Kuruppu et al., (2014)* using three-point-bending tests on semi-circular specimens.

**Table 3: Properties of Kasota Valley Limestone (from *Coldspring Quarry*, retrieved on March 3 from <https://www.coldspringusa.com/quarry>).**

Bulk Density	ASTM C97
Avg. Bulk Density	154 pcf
Absorption	ASTM C97
Avg. Absorption	3.75%
Compressive Strength	ASTM C170
AVG. Compressive Strength	5663 psi
Modulus of Rupture	ASTM C99
AVG. Modulus of Rupture	938 Psi

**Table 4: Materials properties of Kasota Valley Limestone (from *Lu, 2018*)**

	Limestone	Test method
Young's Modulus (Gpa)	45	Uniaxial compression on cylindrical specimens ( <i>ASTM, 2010a</i> )
Possion's Ratio	0.3	Uniaxial compression on cylindrical specimens ( <i>ASTM, 2010b</i> )
Fracture Toughness (Mpa√ m)	0.77	Three-point loading on semicircular bend (SCB) specimens ( <i>Kuruppu et al., 2014</i> )

Specimens were prepared by core drilling (shown in Figure 17a), sawing, and surface grinding (shown in Figure 18a) to obtain 6-inch diameter cylinder at 2.5 inches thickness with flat and parallel faces. These were then core drilled to give either a 0.5-inch or 2-inch central hole. Next a wire saw (Figure 17b) was used to cut two diametrically opposed (bi-wing) notches at 0.3 inches length by 0.27 inches aperture (Figure 18bc).



(a)

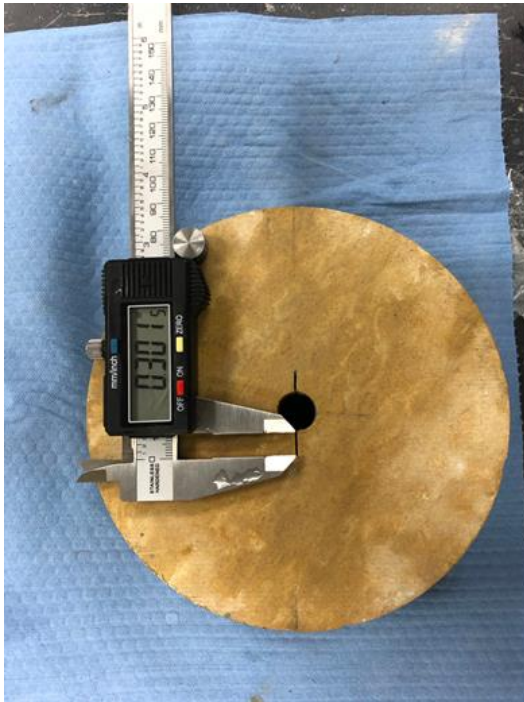


(b)

**Figure 17: (a) Core drilling, (b) wire saw.**



(a)



(b)



(c)

Figure 18: (a) grinding, (b) 0.5-inch limestone specimen, (c) 0.5-inch specimen.

### 3.3 Steps of Burst Experiment

The 0.5-inch and 2-inch central holes give cases with  $w = \frac{b}{a} = 12$  and  $w = \frac{b}{a} = 3$ , respectively. The experiments thus use both stable ( $rw > 1$ ) and unstable ( $rw < 1$ ) configurations (recall global equilibrium criterion, Equation (2-3)). Stable configurations use a 0.5-inch central hole ( $w = 12$ ) with pressure ratios  $r = \frac{P_o}{P_i} = \frac{1}{8}$  and  $r = \frac{1}{6}$ . Unstable configurations use 0.5-inch central hole  $w = 12$  with  $r = 0$  and 2-inch central hole ( $w = 3$ ) with  $r = 0$ ,  $r = \frac{1}{8}$  and  $r = \frac{1}{6}$ .

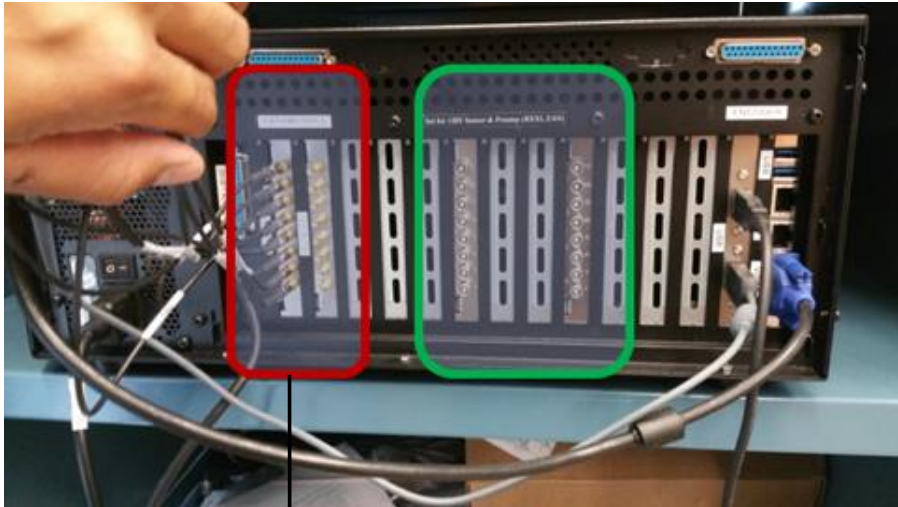
At the beginning of testing, an aluminum spacer was placed in the bottom of the triaxial cell followed by the placement of the limestone specimen. A Tygon tube (recall Figure 16b) with a steel rod inside was placed immediately below the center hole. After that, a second aluminum spacer was put on the specimen through the Tygon tube. A steel plate was placed on the top of the cell and the top rubber plug was right inside this plate to seal the system. Two ISCO syringe pumps were connected, one to the triaxial cell giving confining pressure, and the other to the central tube providing the inner pressure.

After all the preparation work was done, two ISCO syringe pumps were turned on simultaneously and set to pressure ramp rates in order to keep a constant ratio between two pressures. The flow rate and the pressure were monitored until a sudden drop in pressure or increase in flow rate occurred.

### 3.4 Acoustic Emission Detection

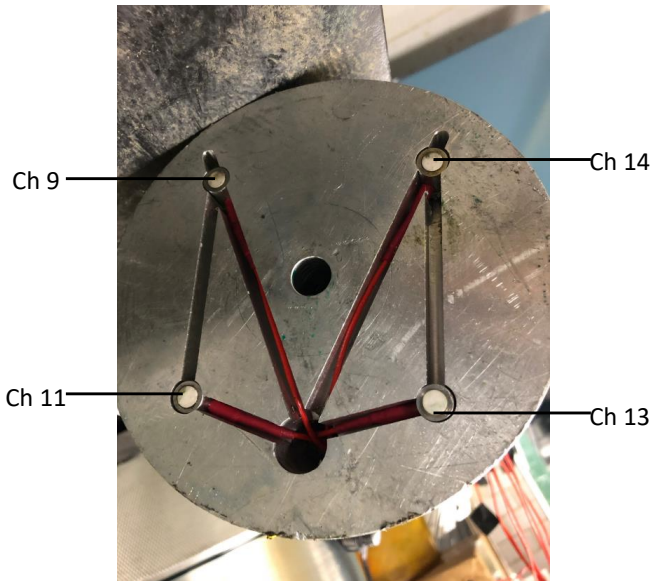
In order to observe if there is evidence of stable crack growth in burst experiment, an Acoustic Emission (AE) detecting system (Figure 19a) was utilized so as to detect the acoustic energy released during rock breakage. It can show evidence of crack growth and other active damage modes in the stressed specimens, including small-scale damage before specimen rupturing, which would provide evidence of stable crack growth prior to macroscopic specimen failure.

Due to access limitations in the burst cell, four sensors were placed only on the bottom surface of top spacer (Figure 19b), thereby contacting the top surface of the specimen. Sensors were distributed as shown in Figure 19(c). Also, as is shown in Figure 19(c), the direction of the notches initiates crack growth between pairs of sensors. Hence, these four sensors work together to detect crack growth, albeit without resolving location in the axial direction of the specimen. The data collected includes a) number of events changing over time, b) location of each event, and c) hit rate. Note that hit rate accounts for every time any channel is triggered by a signal, whereas an event requires 3 channels to receive hits at nearly the same time. Therefore, the results from AE detection can be analyzed along with the pressure records to infer if rock breakage occurred prior to the peak pressure.

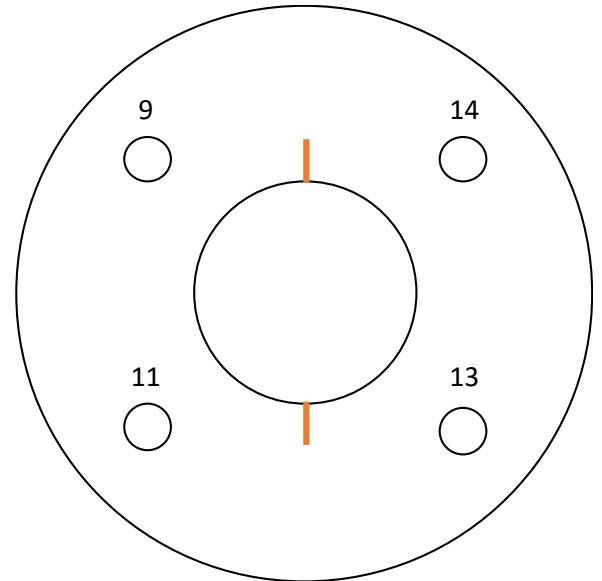


16 channel AE detection card

(a)



(b)



(c)

Figure 19: (a) Acoustic Emission detection system, (b) sensors placed in the bottom spacer, (c) sensor distribution.

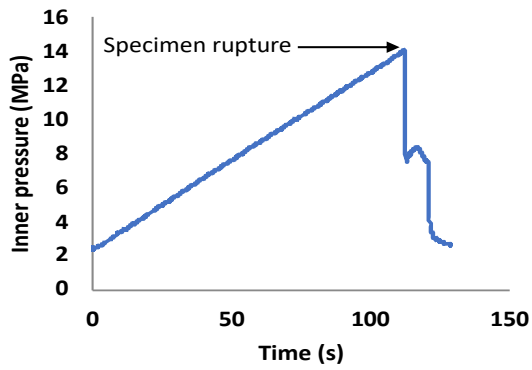
## 4.0 Results of Experiments

### 4.1 Burst Experiments with $w=12$

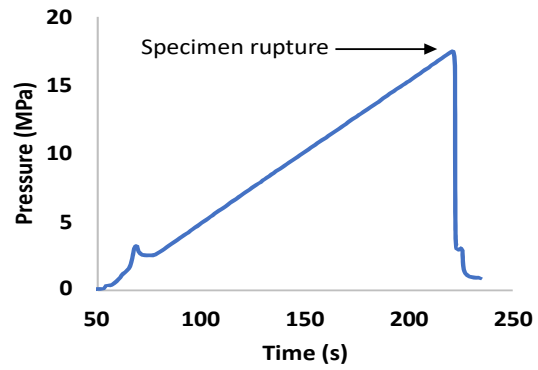
#### 4.1.1 Pressure Records

In the first series of experiments, the geometry configuration is fixed with a 6-inch outer radius and a 0.5-inch inner hole, which means  $w = 12$  (see Table 1). Therefore, all the variables are held the same except only changing  $r$ . Three different pressure ratios have been chosen in these tests, namely  $r = 0$ ,  $r = \frac{1}{8}$  and  $r = \frac{1}{6}$ . Also, two tests are carried out with the AE Detection. To begin with, the inner pressure is increased at a constant rate, 6.2 MPa/min, starting from 2.5 MPa, simultaneously the outer (confining) pressure is increase at 1.03 MPa/min ( $\frac{1}{6}$  of the rate of the inner pressure) from 0.42 MPa, or 0.78 MPa/min ( $\frac{1}{8}$  of the rate of the inner pressure) from 0.31 MPa.

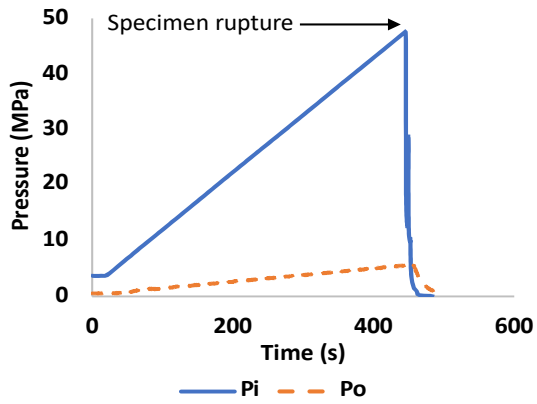
In an example unconfined test ( $r = 0$ , test 1), the inner pressure reaches to 17.5 MPa (shown in Figure 20a), after which the specimen ruptures. This peak pressure is selected as the critical point to estimate the fracture toughness via Equation (2-7). In another typical case with  $r = \frac{1}{6}$  (test 4), the inner pressure ramps up to 50 MPa (shown in Figure 20d), which is selected as the critical pressure to calculate  $K_{IC}$  since the specimen ruptures at this point. As for the example test with  $r = \frac{1}{8}$  (test 3), the peak inner pressure is 47.4 MPa when the specimen begins to rupture. In a word, the critical inner pressure for each test has been selected, corresponding to the pressure drop taken as evidence of specimen's rupture. The resulting estimate of  $K_{IC}$  will be presented in the next chapter.



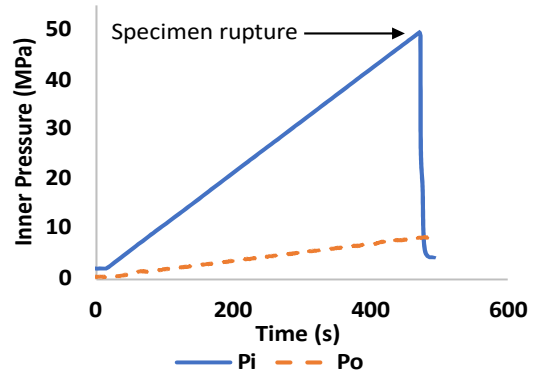
(a)



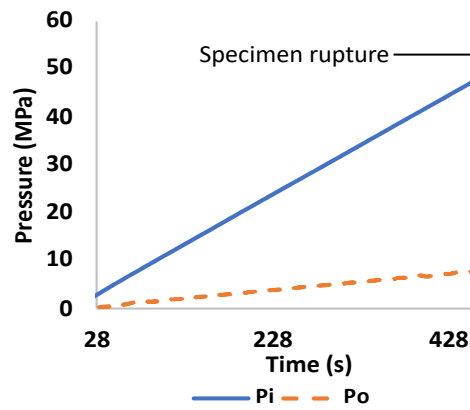
(b)



(c)



(d)



(e)

Figure 20: Pressure records for burst experiments with  $w=12$ , (a) test 1 (unconfined), (b) test 2 (unconfined), (c) test 3 ( $r=1/8$ ), (d) test 4 ( $r=1/6$ ), (e) test 5 ( $r=1/6$ ).

### 4.1.2 AE Records

The modeling (see Chapter 2) and global stability (Equation (2-3)) both predict that there will be stable growth for  $w = 12$  with  $r > 0$ . Hence, tests with  $r = \frac{1}{6}$  and  $\frac{1}{8}$  presented here, which are predicted to have a period of stable growth before specimen rupture. Acoustic Emission (AE) records indicating significant generation of acoustic energy before specimen rupturing will be taken as evidence of stable growth of the crack prior to the rupture. By comparing two series of AE records from one unconfined test (unstable growth, Figure 21) and one confined test with  $r = \frac{1}{8}$  (with predicted stable growth, Figure 21), both with  $w = 12$ , indicate a difference evidencing stable crack growth in the latter case. It is clear that the number of events grows in a different way for these two cases. For the unconfined test, predicted to have only unstable growth, the number of events keeps almost unchanged before specimen rupturing. Then it suddenly increases, corresponding to the pressure drop point shown in Figure 21. But, for the confined test with  $r = \frac{1}{8}$ , with predicted stable growth, the number of events steadily increases from 0 to 250 over a period of about 400 seconds of loading (Figure 22). Then it suddenly grows from 250 to 700, corresponding to the rupture of specimen determined by pressure drop point in Figure 22.

Visible inspection was attempted in order to strengthen the evidence for the existence of stable growth. A test with  $r = \frac{1}{8}$  has been repeated and manually terminated before the rupture. AE records during this test again show steady growth of the event number before the pressure peak. But, before rupture occurs, loading is halted and in order to observe the physical evidence of stable growth, the unruptured specimen was cut into two halves. However, there was no visible trace of stable growth. That is to say, AE records show an obvious difference between stable growth and unstable growth, but it still needs visual proof of the existence of stable fracture growth.

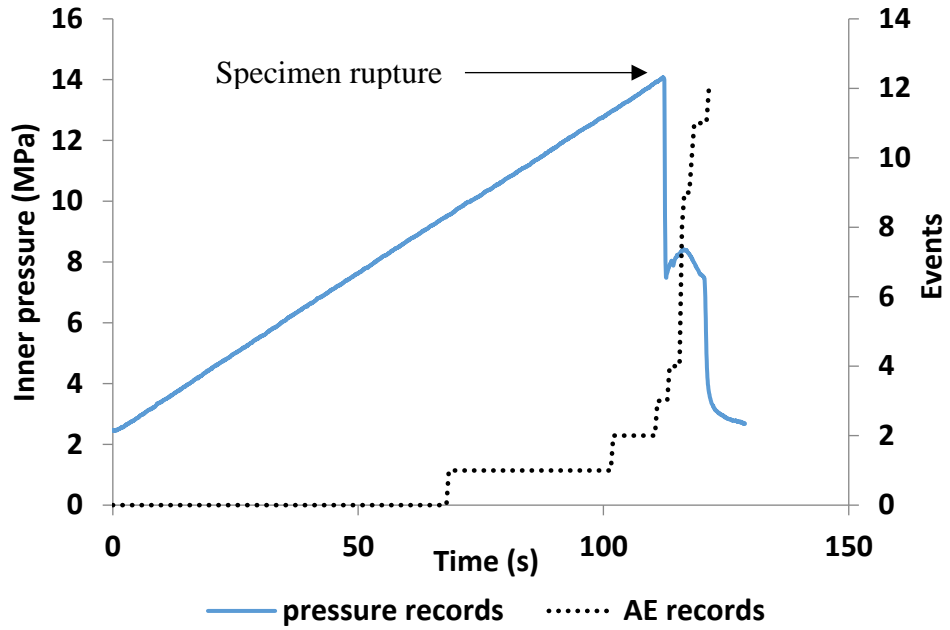


Figure 21: AE records corresponding to test 1 with  $w=12$ ,  $r=0$  (predicted to has only unstable growth).

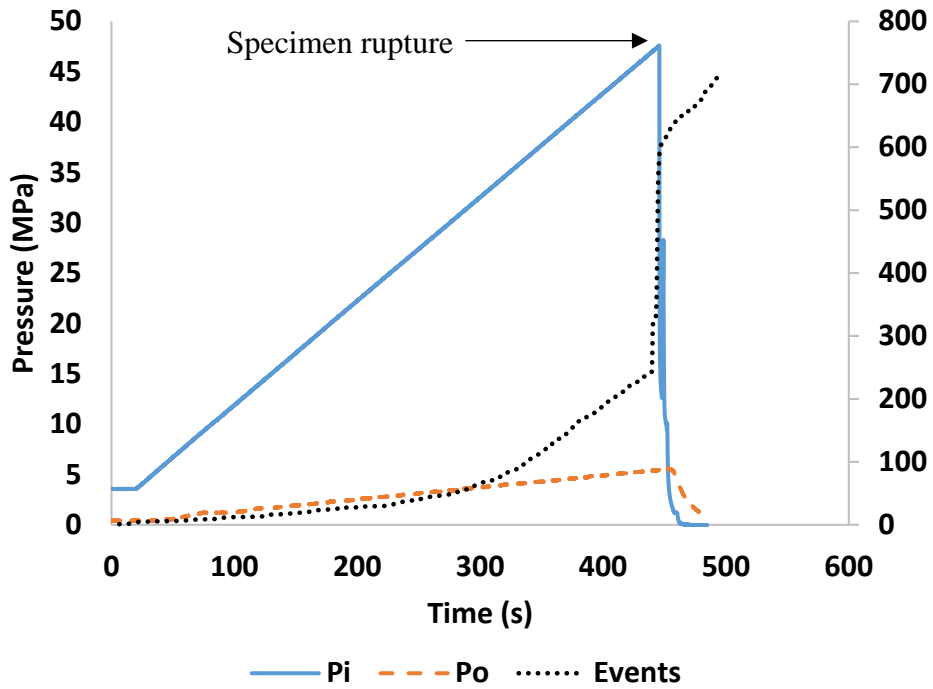


Figure 22: AE records corresponding to test 3 with  $w=12$ ,  $r=1/8$  (with predicted stable growth).

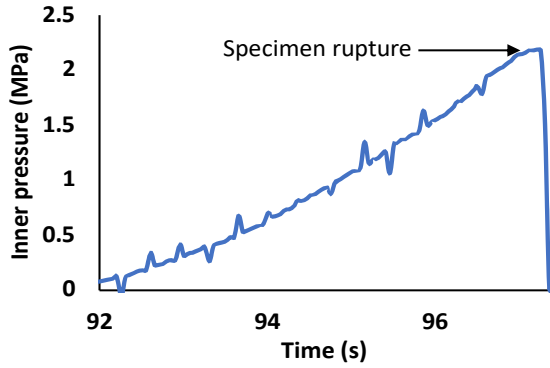
## 4.2 Experiments with $w=3$

### 4.2.1 Pressure Records

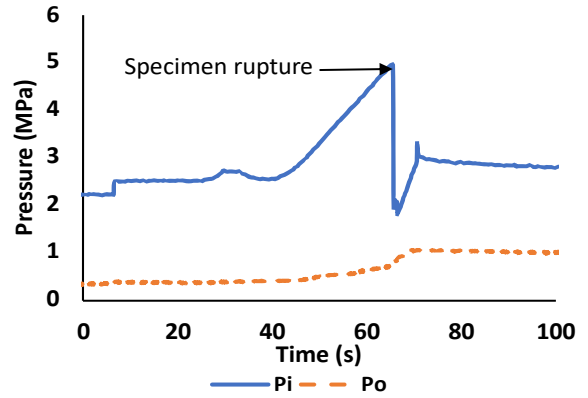
Unlike the tests with  $w = 12$ , the burst experiments with  $w = 3$  are predicted to only have unstable crack growth. This series of burst experiments have been carried out also with different pressure ratios, while all the other variables are controlled the same as before (see Table 1). Hence, being the same as all other tests, the initial inner pressure is 2.48 MPa, and the increasing speed of inner pressure is also fixed as 6.2 MPa/min. Since the configuration  $w$  and initial notch length of each specimen are also fixed, the pressure ratio  $r$  (taken as 0,  $\frac{1}{8}$ , and  $\frac{1}{6}$ ) is the only variable in this series of tests. All the pressure records of experiments designed as in Table 1 are shown in Figure 23.

A typical 2-inch unconfined test ( $r = 0$ , test 6) is shown in Figure 23(a). The inner pressure increased up to 2.2 MPa and then the specimen ruptured from the initial notch. This peak pressure is selected to be the critical pressure to estimate  $K_{IC}$  in the next chapter. Then in a typical 2-inch confined test with  $r = \frac{1}{6}$  (test 9), the outer (confining) pressure was applied with 1.03 MPa/min ( $\frac{1}{6}$  of the rate of the inner pressure) from 0.41 MPa. Finally, the inner pressure increases to 20.8 MPa (Figure 23c), after which the specimen ruptures into 3 pieces (Figure 24). Since Figure 23(c) shows two peaks of inner pressure, it is questionable which one should be chosen to estimate the fracture toughness of the notch. If the second one is chosen,  $K_{IC}$  would be  $2.21 \text{ MPa} \cdot \text{m}^{0.5}$ , which is much larger than results from other similar cases and different experiments like beam tests (Lu, 2018) on the same material. Therefore, the first peak is selected to be the critical point to estimate  $K_{IC}$ . A possible interpretation for a third fracture is that the specimen failed along the notch in one

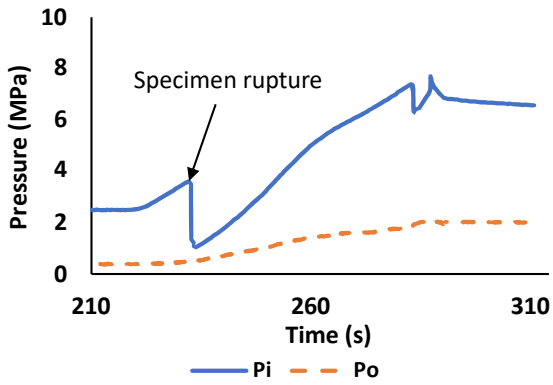
direction at the first peak, after which it broke 90 degrees from the initial breakage at the second peak. Afterwards, it failed at the second notch and the specimen subsequently became unstable (not satisfying global force equilibrium, as described in Section 2). To test the hypothesis, two more tests have been repeated. Since the similar phenomenon shows up again and after trying to calculate  $K_{IC}$  using each pressure peak, our hypothesis seems to be supported that the first peak corresponds to initial growth and should be used to compute  $K_{IC}$ .



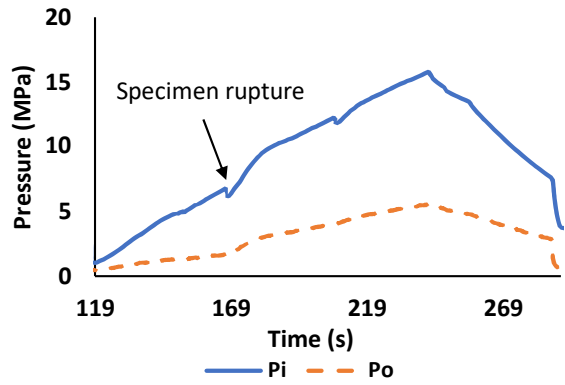
(a)



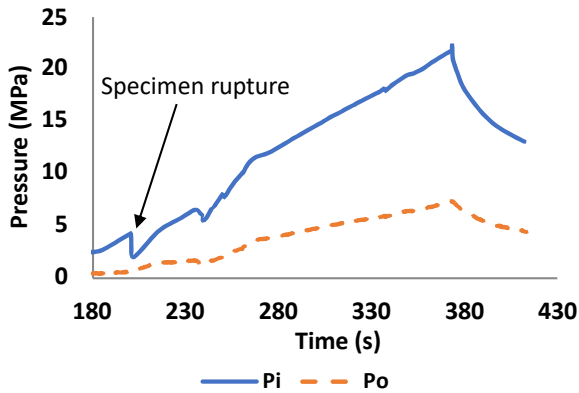
(b)



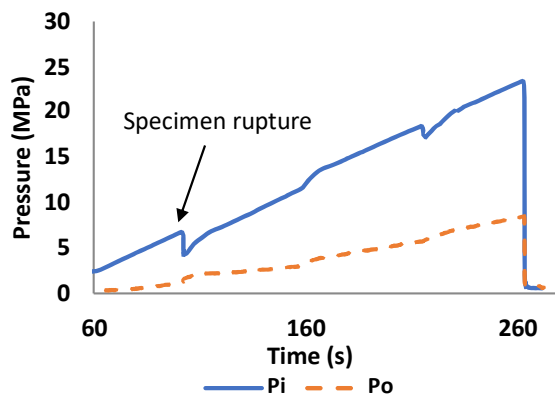
(c)



(d)



(e)



(f)

Figure 23: Pressure records for burst experiments with  $w=3$  (2-inch hole), (a) test 6 (unconfined), (b) test 8 ( $r=1/8$ ), (c) test 9 ( $r=1/6$ ), (d) test 10 ( $r=1/6$ ), (e) test 11 ( $r=1/6$ ), (f) test 12 ( $r=1/6$ ).



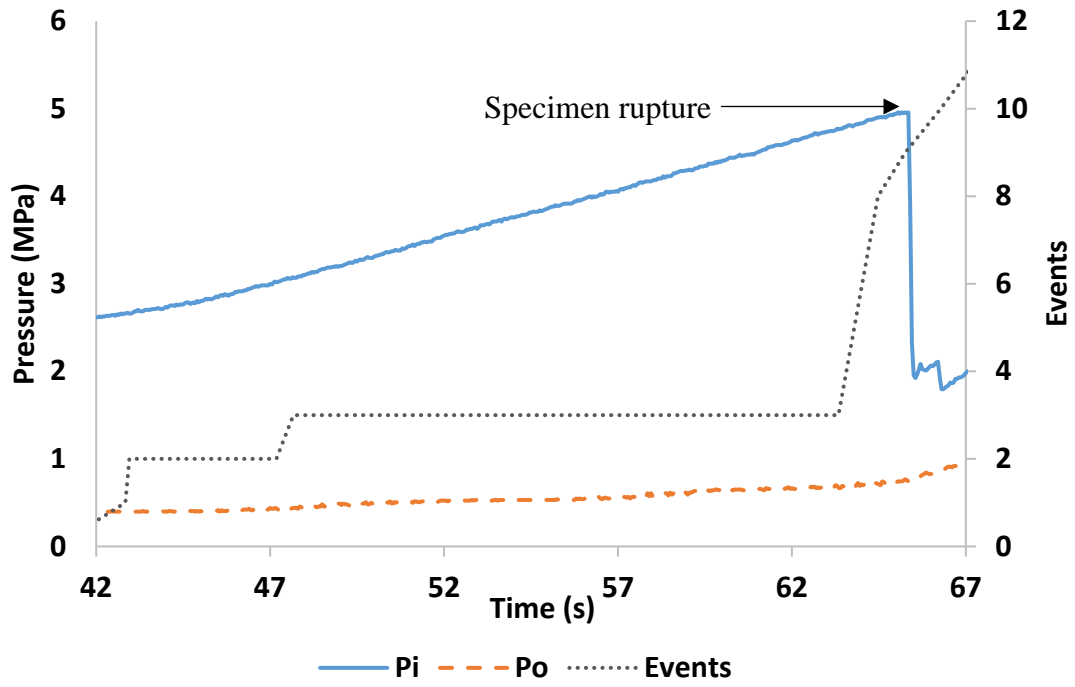
Figure 24: Specimen from test 12 after test with a third crack.

#### 4.2.2 AE Records

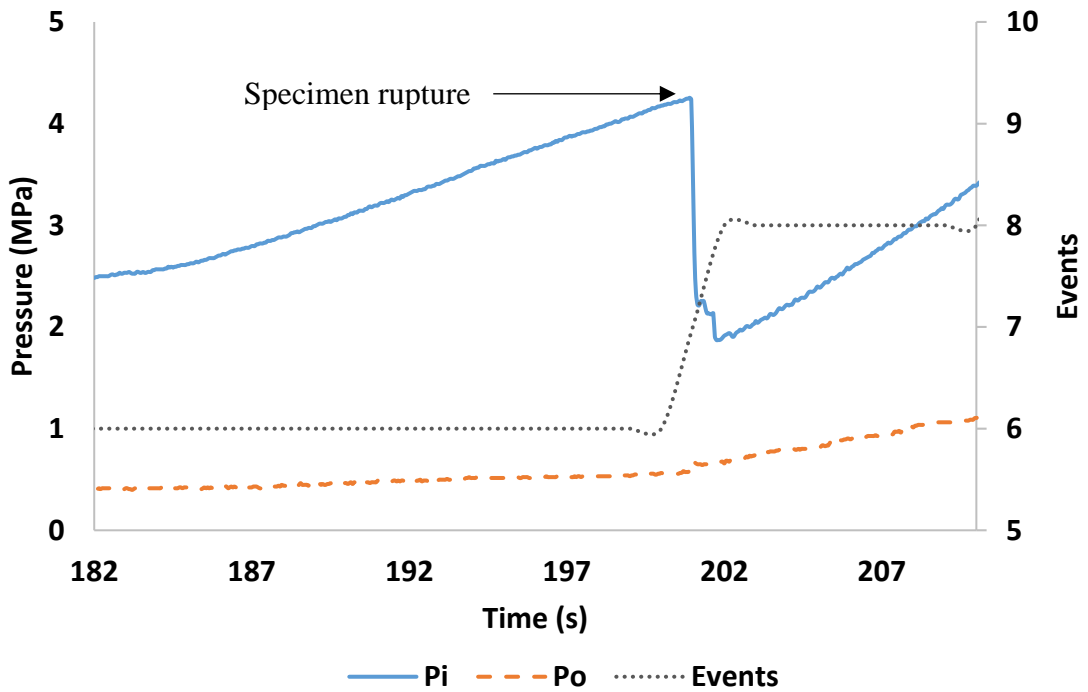
The AE records in burst experiments with  $w = 12$  present some differences between unstable growth and stable growth (recall Figure 21, Figure 22). For tests with 2-inch hole size, both the SIF calculation and global equilibrium criterion predict that there will only be unstable growth in these tests with  $r = 0$ ,  $\frac{1}{8}$  and  $\frac{1}{6}$ . Hence it is useful to observe characteristics of unstable growth in these AE records to compare to those previous tests with possible stable growth.

In two tests with  $r = \frac{1}{8}$  (test 8) and  $r = \frac{1}{6}$  (test 12) for  $w = 3$ , the peak inner pressures have been selected to be 4.96 and 4.24 MPa, after which the specimen ruptures into two parts. The AE records show a similar behavior to the previous test with only unstable growth when  $w = 12$  (0.5-inch hole) and  $r = 0$ . In detail, in the case with  $w = 3$  and  $r = \frac{1}{8}$  (test 8) when the pressure

increases before specimen rupturing, the number of events stays around 3 for 20 seconds until a sudden pressure drop occurs (Figure 25a). Then the number of events increases to over 10 suddenly (Figure 25a). And in the case with  $r = \frac{1}{6}$  (test 12) when the pressure is ramping up before the first peak (Figure 25b), the number of events remains almost unchanged at 6 for 20 seconds then suddenly goes up to 8 (Figure 25b), corresponding to the pressure drop. These results further show the feature of test with unstable growth from AE using a different geometry configuration. That being said, the cause of the few events that occurred at the early time is unclear and it cannot be ruled out that it could be associated with unexpected stable crack growth.



(a)



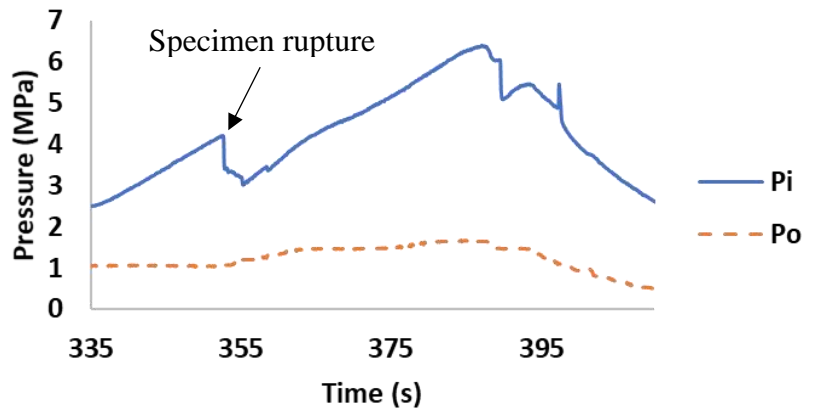
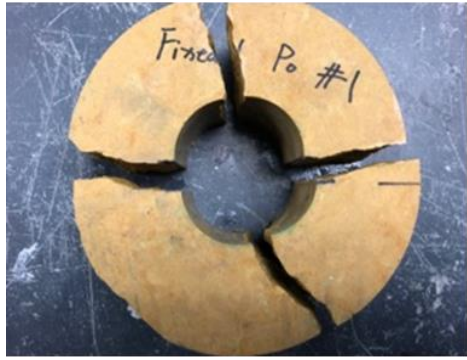
(b)

Figure 25: AE records corresponding to burst experiments with  $w=3$  (a)  $r=1/8$  (test 8), (b)  $r=1/6$  (test 12).

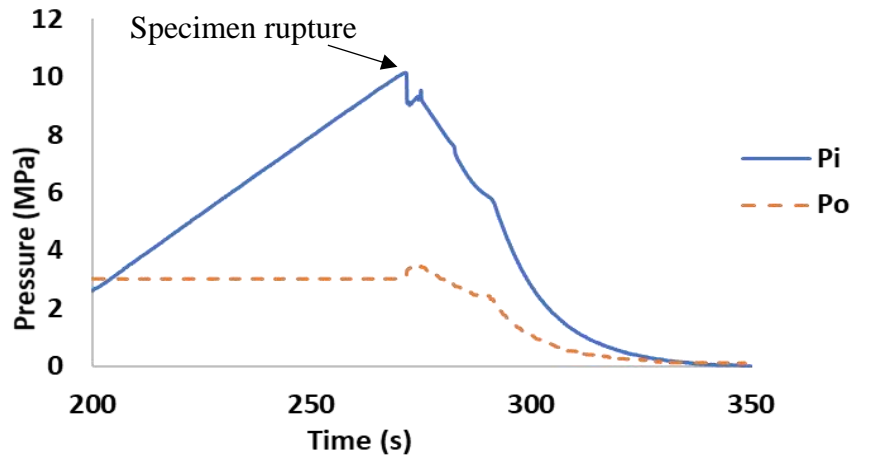
### 4.3 Fixed Confinement Tests

The outer and inner pressure of the original burst experiment (*Abou-Sayed, 1978*) increases with a constant ratio  $r$ . In previous tests, both the initial inner pressure and the initial notch length are fixed. Then those tests are designed to analyze the dependence of pressure ratio  $r$  and the specimen configuration  $w$ . In this part, a series of tests with fixed confinement have been carried out to further evaluate the possible stress dependence of the behavior from another perspective.

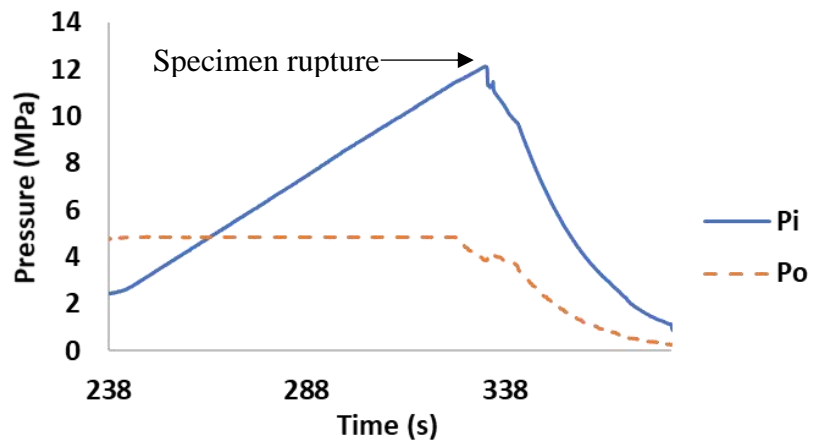
Three levels of outer pressure have been applied for tests with the same geometry ( $w = 3$ ), namely 1 MPa, 3 MPa and 4.8 MPa. The specimens after the tests and the pressure monitoring results are shown in Figure 26(a) and Figure 26(c). Being similar to burst experiments with  $w = 3$ , when the confining stress was larger than 3 times of inner pressure, the specimen was globally stable and there was no third or fourth fracture appearing. This observation is consistent with the single pressure drop in Figure 26(c, e). The first peaks, which have been chosen to be the critical points to estimate the  $K_{IC}$ , are 4.07 MPa, 9.71 MPa and 11.55 MPa, respectively.



(a)



(b)



(c)

Figure 26: Tests with fixed confinement as, (a) 1 MPa (test F-1), b) 3 MPa (test F-2), c) 4.8 MPa (test F-3).

## 5.0 Discussion

### 5.1 Estimates of Fracture Toughness

#### 5.1.1 $K_{IC}$ Calculation

The fracture toughness for the burst experiment is determined by critical pressure and geometry. Using the SIF computed as described in Chapter 2. The critical inner pressure point has been identified for each test, as described in Chapter 4. In this chapter,  $K_{IC}$  is estimated for each situation using Equation (2-7), with the results shown in Table 5. Also, for the tests with fixed confinement,  $K_{IC}$  is shown in Table 6. It is clear that  $K_{IC}$  varies significantly from  $0.34 \text{ MPa}\sqrt{\text{m}}$  to  $1.55 \text{ MPa}\sqrt{\text{m}}$ . Connecting this variation to geometry and loading is the main topic of discussion in this chapter.

**Table 5: Summary of parameters and  $K_{IC}$  calculation for all tests (note stability is determined by “rw” criterion, see Equation (2-3); “AE” means this test is under AE detection).**

Test Name	Stability	Hole size (in)	w=b/a	r=Po/Pi	rw	Pi (MPa)	K <sub>IC</sub> (MPa√m)
1	unstable	0.5	12	0	0	14.1	0.84
2, AE	unstable	0.5	12	0	0	14.0	0.84
3, AE	stable	0.5	12	1/8	1.5	47.6	1.55
4	stable	0.5	12	1/6	2	49.7	1.21
5	stable	0.5	12	1/6	2	52.2	1.28
6	unstable	2	3	0	0	2.6	0.43
7	unstable	2	3	0	0	2.2	0.36
8, AE	unstable	2	3	1/8	0.375	5.0	0.60
9	unstable	2	3	1/6	0.5	6.9	0.74
10	unstable	2	3	1/6	0.5	7.4	0.79
11	unstable	2	3	1/6	0.5	6.8	0.73
12, AE	unstable	2	3	1/6	0.5	6.6	0.70

**Table 6: Summary of parameters and  $K_{IC}$  calculation for fixed confinement tests.**

Tests Name	Stability	Pi (MPa)	Fixed Po (MPa)	w	r	rw	K <sub>IC</sub> (MPa√m)
F-1	unstable	4.21	1	3.00	0.24	0.71	0.35
F-2	unstable	10.09	3	3.00	0.30	0.89	0.64
F-3	stable	11.87	4.8	3.00	0.40	1.21	0.34

### 5.1.2 Configurational Dependence

This section presents analysis of the configurational dependence of  $K_{IC}$ . All the results of  $K_{IC}$  are summarized in Figure 27. Since there are two independent variables in the experiments, pressure ratio  $r$  and radius ratio  $w$ , the x axis is set to be  $r$ , and the tests with different  $w$  are divided into two groups.

On the one hand, we focus on the calculated results in each group with the same hole size. In the group of tests with  $w = 3$ , which has only unstable growth, presenting a linear positive correlation between  $K_{IC}$  and  $r$ . However, in the group with  $w = 12$ , the correlation is not apparent, which might be due to the stable growth.

On the other hand, when comparing the results between each pair of tests with the same  $r$  but the different  $w$ , the dependence on  $r$  and  $w$  can be observed. In detail, tests with smaller hole size (larger  $w$ ) lead to a larger value of calculated  $K_{IC}$ . Even in the unconfined test ( $r = 0$ ),  $K_{IC}$  calculated from 0.5-inch hole set-up ( $w = 12$ ) is about twice the  $K_{IC}$  from 2-inch hole set-up ( $w = 3$ ).

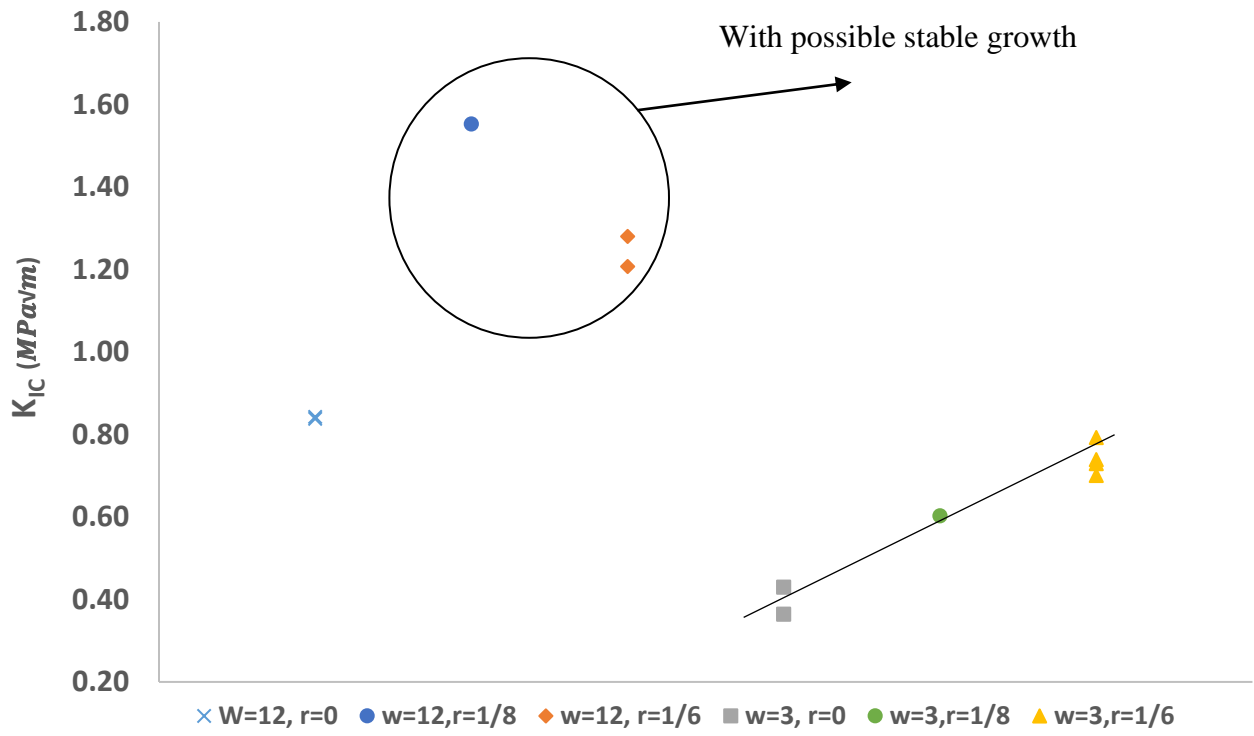


Figure 27: Results of  $K_{IC}$  calculation for all tests.

## 5.2 Dependence of Fracture Toughness on Confinement

### 5.2.1 Stable Tests

Recall the past burst experiments have led to a belief that  $K_{IC}$  depends upon confining stress (Figure 1). This section examines the possible dependence of  $K_{IC}$  on confinement in 0.5-inch burst experiment with possible stable growth. With all other variables the same except confinement, it is firstly observed that the values of  $K_{IC}$  calculated from all confined tests are over 50% larger than the unconfined ones. For example,  $K_{IC}$  of the test with  $r = \frac{1}{8}$  is larger than that of the test with  $r = \frac{1}{6}$ , which is contrary to results from 2-inch tests. Unlike the results from previous published research, which presents a linear positive correlation between  $K_{IC}$  and confining stress (see Figure 1), the results from these tests show an unanticipated behavior, which is a negative correlation, i.e., In detail, when the confining pressure is large enough, a negative correlation occurs (Figure 28a). If the global equilibrium criterion is used to analyze this phenomenon, this trend is clearly in the range of  $rw > 1$  (stable growth condition), as shown in Figure 28(b).

Taking all these results into account, the dependence of fracture toughness on confinement in stable tests are hard to interpret. But these results could be another evidence of difficulty arising from stable fracture growth. It is consistent with the hypothesis that the stable growth will lead to inaccurate estimation of fracture toughness.

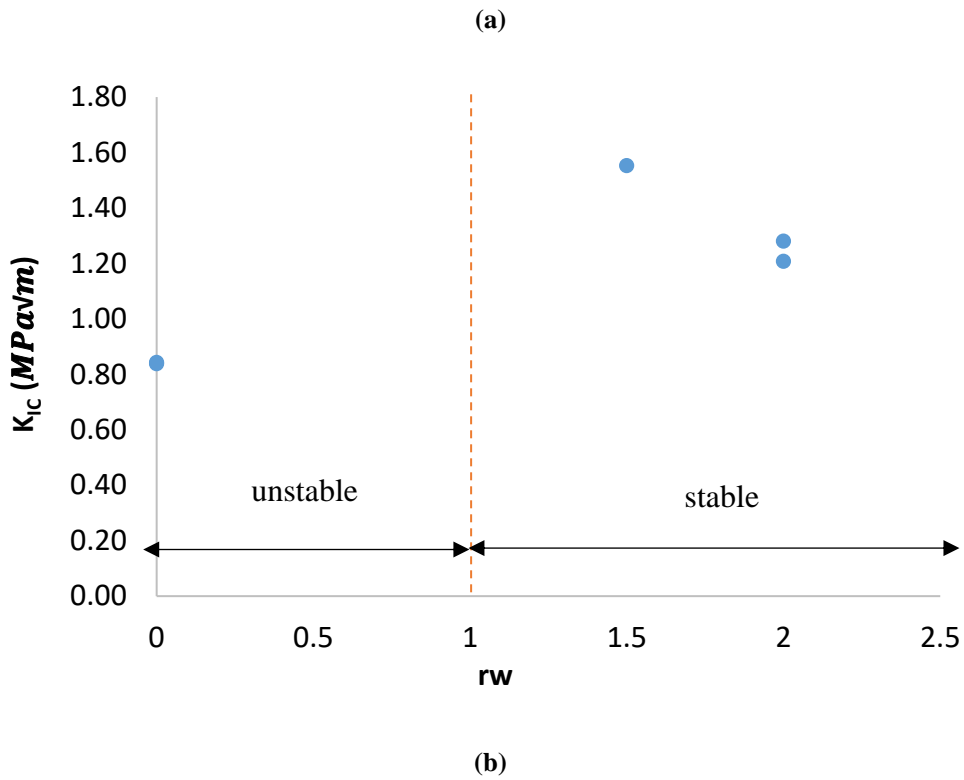
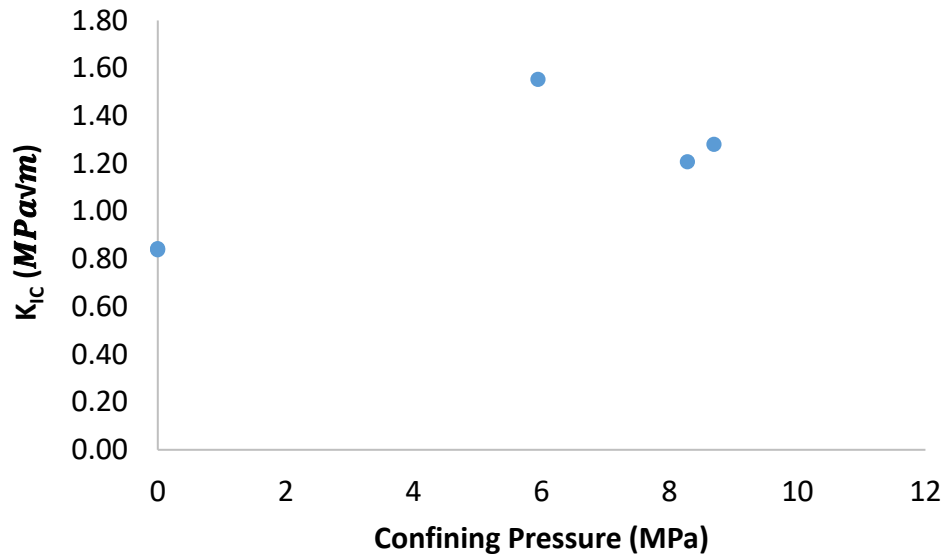
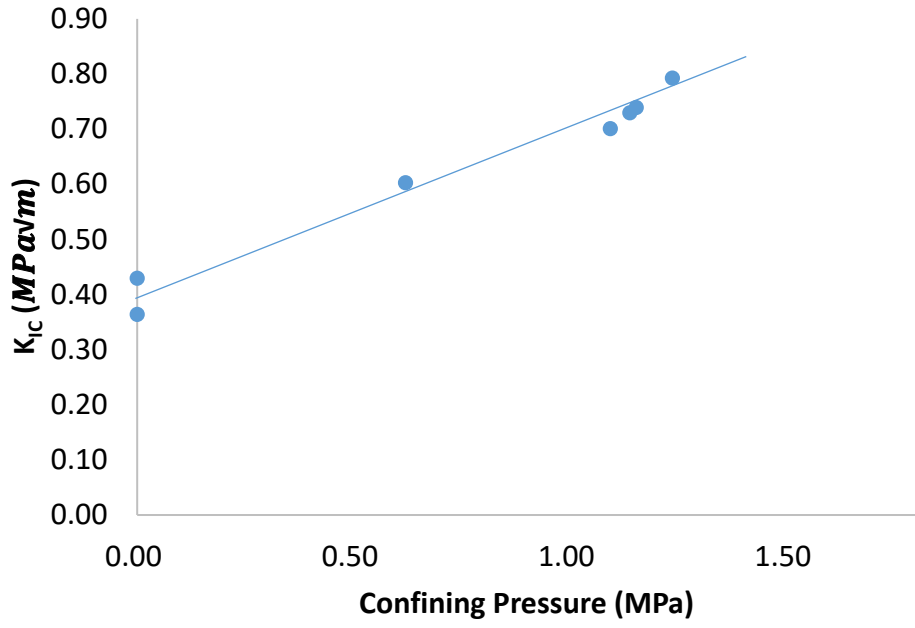


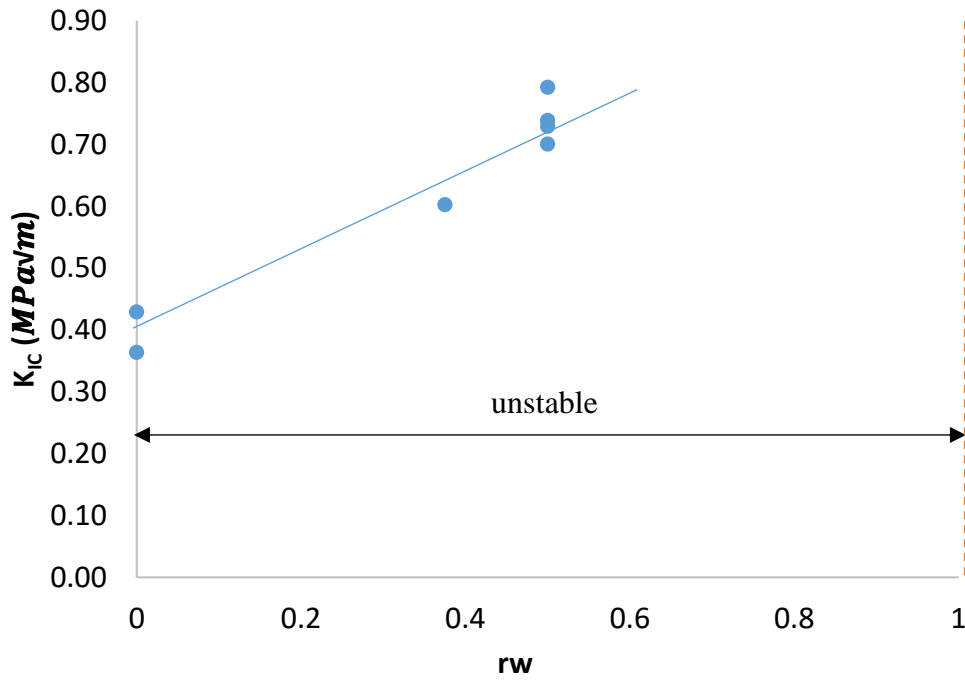
Figure 28: Results from burst experiment with  $w=12$ , (a)  $K_{IC}$  versus confining pressure, (b)  $K_{IC}$  versus  $rw$  (global equilibrium criterion, see Equation (2-3)).

### 5.2.2 Unstable Tests

The dependence of  $K_{IC}$  on confinement appears more clearly in the burst experiment with  $w = 3$  (2-inch hole). It is consistent with the published results that  $K_{IC}$  has a linear positive correlation with the confining stress, as shown in Figure 29(a). Recall modeling and the AE records show that there is only unstable growth in this series of tests. Also, all these tests are in the range of  $rw < 1$  (shown in Figure 29b), which is proposed to be unstable condition in the global equilibrium criterion (see Chapter 2, Equation (2-3)). In addition, when looking back to pressure records in Figure 23, there is a trend toward the global force equilibrium ( $rw = 1$ ) after the rupture in these tests. Taken together, the evidence points to only unstable growth in this series, which, in turn, shows a clear positive correlation between  $K_{IC}$  and confinement.



(a)



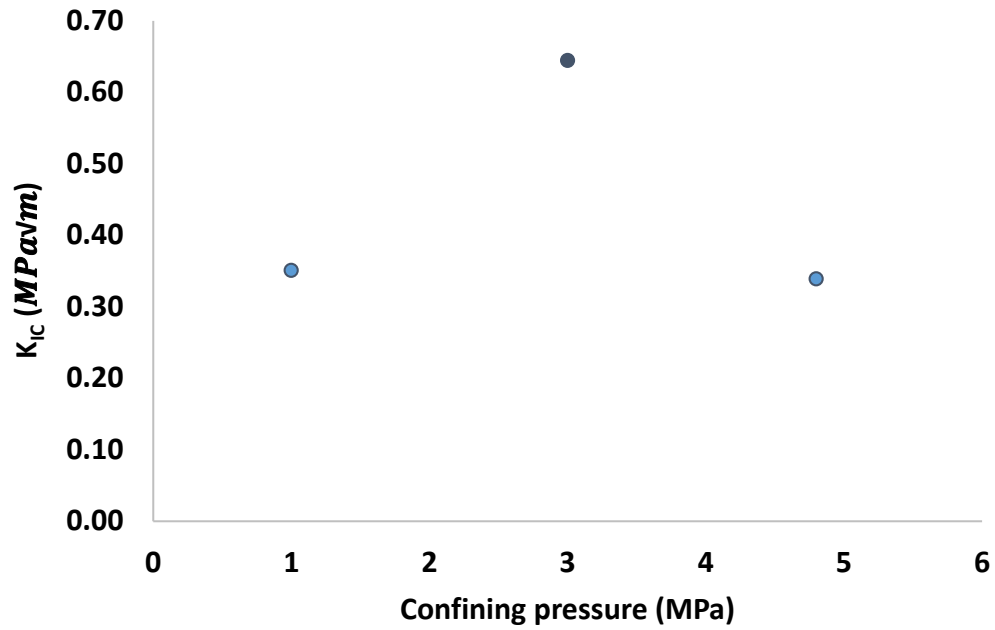
(b)

Figure 29: Results from burst experiment with  $w=3$ , (a)  $K_{IC}$  versus confining pressure, (b)  $K_{IC}$  versus  $rw$  (global equilibrium criterion, see Equation (2-3)).

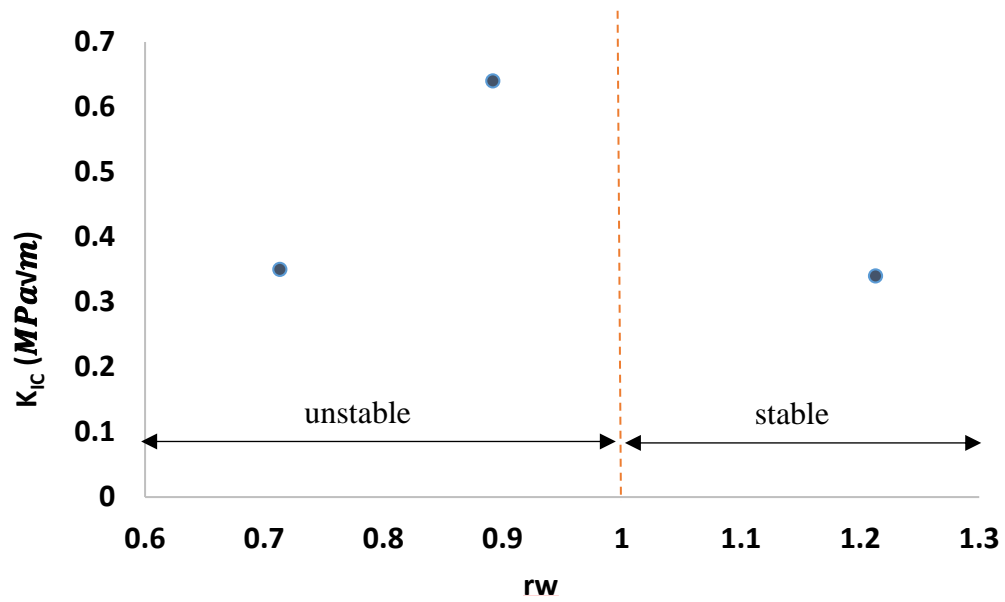
### 5.2.3 Fixed Confinement Tests

In this part, the dependence of  $K_{IC}$  on confinement will be discussed using results from fixed confinement tests. Recall that there are three values of confining pressure applied for these tests with the same configuration ( $w = 3$ ), namely 1 MPa, 3 MPa and 4.8 MPa. The  $K_{IC}$  for each test has been calculated respectively, as  $0.35 \text{ MPa} \cdot \text{m}^{0.5}$ ,  $0.64 \text{ MPa} \cdot \text{m}^{0.5}$  and  $0.34 \text{ MPa} \cdot \text{m}^{0.5}$ , as shown in Figure 30(a). An unanticipated phenomenon shows up again that when confining stress is getting large enough, the  $K_{IC}$  decreases, which is similar to the results from 0.5-inch burst experiments. This phenomenon possibly can be explained using the global equilibrium criterion (see Equation (2-3)). Figure 30(b) shows that the first two tests are in the range of  $rw < 1$ , which leads to a linear positive correlation between the fracture toughness and the confining stress. However, the last test, falling in the range of  $rw > 1$ , shows a downward trend. This is consistent with tests with the possible stable growth.

These results further strengthen the previous argument that when confining stress is large enough ( $rw > 1$ ), the dependence of  $K_{IC}$  on confinement will be difficult to interpret, which is possibly due to the stable growth causing inaccurate estimation of  $K_{IC}$ . In contrast, in the range of  $rw < 1$ , there appears to be a linear positive correlation between  $K_{IC}$  and confining pressure.



(a)



(b)

Figure 30: Results from fixed confinement tests, (a)  $K_{IC}$  versus confining pressure, (b)  $K_{IC}$  versus  $rw$  (global equilibrium criterion, see Equation (2-3)).

### 5.3 Summary of Recommendations

The recommendations for future application and research using burst experiments are as follows:

1. It is desirable to use unstable configurations ( $rw < 1$ ). Otherwise, there is potential for inaccurate estimation of  $K_{IC}$  in general including a possibility of spurious dependence of fracture toughness on confining stress. Additionally, the global equilibrium criterion (Equation (2-3)) is found to be valid to classify the situations by comparing the radius ratio  $w$  and the pressure ratio  $r$  (inner over outer). When  $rw > 1$ , there is possible stable fracture growth before rupture, which leads to inaccurate estimation of the fracture toughness.

2. It is necessary to further investigate the existence of stable growth. Some clues could be found by artificially terminating a burst experiment right before the rupturing point, and then the specimen should be cut layer by layer, which would comprise a more comprehensive search than what carried out here. If some visible evidence can be observed, the existence of stable growth can be more conclusively determined.

3. A 3D distribution of sensors should be used to get more information from AE detection. More compelling evidence of the pre-existing stable growth would be found if locations were reliable and, better yet, if moment tensor analysis (*Shigeishi and Ohtsu, 2001*) could be carried out on the AE.

4. Practically, it is better to use larger hole size when performing burst experiment since the small hole size will lead to higher overall pressures during the test. This higher pressure leads to higher test failure rates.

## 6.0 Conclusion

This research is aimed at identifying stable crack growth in the burst experiment, demonstrating its consequences, and proposing modification for overcoming the problems it creates. Additionally, this research studies the dependence of fracture of rock on confinement.

The main contributions of this thesis are as follows:

1. Evidence of stable growth of fracture has been found out from two aspects. One is the features of AE detection records. In general, the records from predicted stable growth tests are different from the tests predicted to have only unstable growth. Firstly, the number of events is much larger than those in only unstable growth situation. Also, there is a steadily increasing trend of events versus time in the stable growth tests. Finally, there is a downward trend in stable tests for  $K_{IC}$  versus confinement, which could be due to stable crack growth.

2. The dependence of  $K_{IC}$  on confinement has been analyzed with both proportional pressurized and fixed confinement tests. In the tests with only unstable growth (when  $rw < 1$ ), there is a linear positive correlation between  $K_{IC}$  and confining pressure. But in the tests with stable crack growth, it is difficult to interpret this dependence. In detail, a negative correlation is always appearing when the confining stress is large enough, such that  $rw > 1$  (stable condition).

3. A criterion of stability based on global force equilibrium has been proposed and tested (see Equation (2-3)). It is shown to be effective for determining the growth regime. If  $rw < 1$ , there will be only unstable crack growth. Otherwise in the range of  $rw > 1$ , the stable crack growth is predicted to exist, which can lead to an inaccurate estimation of  $K_{IC}$ .

In summary, AE records show evidence of stable growth prior to specimen rupture, leading to inaccurate estimation of  $K_{IC}$  and unclear dependence of  $K_{IC}$  on confinement. But for the

unstable cases, there is a linear positive correlation between  $K_{IC}$  and confining pressure. The global equilibrium criterion is able to predict the stability of burst experiment. The future research can use this criterion to design burst experiment and then use advanced analyses of AE results, experimentation on other rocks as well as more ideally brittle materials such as glass and paused stable experiments with detailed serial sectioning. All of these extensions would bring clarity to the nature of the stable growth as well as to better understand a deeper, more long-standing question around the mechanical origin and a priori prediction of stress dependence of rock fracture toughness.

## Bibliography

- Abou-Sayed, A. S. (1978). An experimental technique for measuring the fracture toughness of rock under downhole stress condition. VDI-berichte, 313, 819-824.
- Abou-Sayed, A. S., & Jones, A. H. (1979). U.S. Patent No. 4,152,941. Washington, DC: U.S. Patent and Trademark Office.
- Bowie, O. L., & Freese, C. E. (1972). Elastic analysis for a radial crack in a circular ring. Engineering Fracture Mechanics, 4(2), 315-321.
- Clifton, R. J., Simonson, E. R., Jones, A. H., & Green, S. J. (1976). Determination of the critical-stress-intensity factor K<sub>IC</sub> from internally pressurized thick-walled vessels. Experimental Mechanics, 16(6), 233-238.
- Coldspring Quarry. Kasota Valley Limestone. Retrieved March 2, 2019, from <https://www.coldspringusa.com/building-materials/products-colors-and-finishes/limestone/kasota-valley-limestone/>
- Fialko, Y. A., & Rubin, A. M. (1997). Numerical simulation of high - pressure rock tensile fracture experiments: Evidence of an increase in fracture energy with pressure. Journal of Geophysical Research: Solid Earth, 102(B3), 5231-5242.
- Geniaut, S., Massin, P., & Moës, N. (2005). Evaluation of stress intensity factors with G-Theta method and level sets in Code\_Aster. In ICF11, 2005, Turin, Italy.
- Griffith, A. (1924). The theory of rupture. In First Int. Cong. Appl. Mech (pp. 55-63).
- Hashida, T., Oghikubo, H., Takahashi, H., & Shoji, T. (1993). Numerical simulation with experimental verification of the fracture behavior in granite under confining pressures based on the tension-softening model. International Journal of Fracture, 59(1), 227-244.
- Holder, J., Morita, N., Kenrick, A. J., Thallak, S., & Gray, K. E. (1993). Measurements of effective fracture toughness values for hydraulic fracture: Dependence on pressure and fluid rheology. In SPE Production Operations Symposium. 21-23 March, Oklahoma City, Oklahoma
- Irwin, G. (1957). Analysis of stresses and strains near the end of a crack transversing a plate. Trans. ASME, Ser. E, J. Appl. Mech., 24, 361-364.
- K. Yoshioka, Y. Zhang, A. Bungler, J. Adachi, A. El-Fayoumi, B. Bourdin (2019). Revisiting the fracture toughness of rocks under confining pressure. (in preparation).

- Ko, T. Y., & Kemeny, J. (2007). Effect of confining stress and loading rate on fracture toughness of rocks. In 1st Canada-US Rock Mechanics Symposium. American Rock Mechanics Association. 27-31 May, Vancouver, Canada.
- Kuruppu, M. D., Obara, Y., Ayatollahi, M. R., Chong, K. P., & Funatsu, T. (2014). ISRM-suggested method for determining the mode I static fracture toughness using semi-circular bend specimen. *Rock Mechanics and Rock Engineering*, 47(1), 267-274.
- Lu, G. (2018). Hydraulic Fracture Initiation and Propagation under subcritical conditions (Doctoral dissertation, University of Pittsburgh).
- Orowan, E. (1952). Fundamentals of brittle behavior in metals. *Fatigue and fracture of metals*, 3, 139-167.
- Rice, J., Paris, P., & Merkle, J. (1973). Some further results of J-integral analysis and estimates. *ASTM special technical publication*, (536), 231-245.
- Roegiers, J. C., & Zhao, X. L. (1991). Rock fracture tests in simulated downhole conditions. In *The 32nd US Symposium on Rock Mechanics (USRMS)*. American Rock Mechanics Association. 10-12 July, Norman, Oklahoma.
- Rubin, A. M. (1993). Tensile fracture of rock at high confining pressure: implications for dike propagation. *Journal of Geophysical Research: Solid Earth*, 98(B9), 15919-15935.
- Schmidt, R. (1977). Effect of confining pressure on fracture toughness of Indiana limestone. *International Journal of Rock Mechanics and Mining Sciences & Geomechanics Abstracts*, 14, 289-293.
- Shigeishi, M., & Ohtsu, M. (2001). Acoustic emission moment tensor analysis: development for crack identification in concrete materials. *Construction and Building Materials*, 15(5-6), 311-319.
- Stauffer, Clinton R.; Thiel, George A. (1933). Bulletin No. 23. The Limestones and Marls of Minnesota. Minnesota Geological Survey. Retrieved from the University of Minnesota Digital Conservancy, <http://hdl.handle.net/11299/56631>.
- Thallak, S. G., Holder, J., & Gray, K. E. (1993). The pressure dependence of apparent hydrofracture toughness. In *The 34th US Symposium on Rock Mechanics (USRMS)*. American Rock Mechanics Association. 28-30 June, Madison, Wisconsin.
- Thiercelin, M. (1989). Fracture toughness and hydraulic fracturing. In *International Journal of Rock Mechanics and Mining Sciences & Geomechanics Abstracts* (Vol. 26, No. 3-4, pp. 177-183). Pergamon.